IEEE Access
Multidisciplinary | Rapid Review | Open Access Journal

Received August 25, 2020, accepted September 7, 2020, date of publication September 14, 2020,
date of current version September 25, 2020.

Digital Object Identifier 10.1109/ACCESS.2020.3023815

Estimation of the Time-Variant Velocity of a Single Walking Person in Two-Dimensional Non-Stationary Indoor Environments Using Radio-Frequency Techniques

RYM HICHERI[1], (Member, IEEE), MATTHIAS PÄTZOLD[1], (Senior Member, IEEE), AND NÉJI YOUSSEF[2]

[1]Faculty of Engineering and Science, University of Agder, 4898 Grimstad, Norway
[2]Ecole Supérieure des Communications de Tunis, Université de Carthage, Ariana 2083, Tunisia

Corresponding author: Rym Hicheri (rym.hicheri@uia.no)

This work was supported by the Research Council of Norway through the WiCare Project under Grant 261895/F20.

ABSTRACT Accurate estimation of the time-variant (TV) velocity of moving persons/objects in indoor spaces is of crucial importance for numerous wireless indoor applications. This article introduces a novel iterative procedure to estimate the TV velocity, i.e., TV speed and TV angle-of-motion (AOM), of a single moving person in 2D indoor environments by using radio-frequency (RF) techniques. The indoor area is equipped with a distributed 2×2 multiple-input multiple-output (MIMO) system. The proposed method is divided into two parts. In the first part, we estimate the path gains and the instantaneous Doppler frequencies by fitting the exact spectrograms of the complex channel gains of a 2D non-stationary channel model to the spectrograms obtained from the received radio signals. In the second part of this work, another estimation procedure is proposed to deduce the desired TV velocity from the estimated TV Doppler frequencies. Although, the primary objective of the proposed iterative estimation techniques is to determine the TV velocity, i.e., TV speed and TV AOM, of the walking person, it computes all channel parameters including the path gains, the TV angles-of-arrival, and the TV angles-of-departure. Closed-form solutions are derived for the path gains, the TV Doppler frequencies, the TV speed, and the TV angles, which in turn reduces considerably the complexity of the optimization methods. Numerical results are provided to demonstrate the validity and robustness of the proposed algorithms against noise. This is accomplished by analyzing the agreement between the estimated parameters of interest with the corresponding exact values, which are known from computer generated test signals. The estimation accuracy of the proposed method is evaluated for different values of the signal-to-noise (SNR) ratio. It is shown that this technique estimates the TV Doppler frequencies and TV speed with an accuracy between 70 % and 97 % for SNR values ranging from 0 dB to 20 dB.

INDEX TERMS Human activity of daily life, non-stationary indoor channels, Doppler characteristics, time-variant velocity estimation, distributed multiple-input multiple-output systems.

I. INTRODUCTION

Human activity monitoring aims at capturing and identifying the motion and activities of persons using vision-based approaches, sensing techniques, or radio signal analysis methods. This is an ongoing research topic that has gained a huge amount of attention in the last decade due to its emerging applications in, for example, surveillance, robotics, and healthcare. Within the context of healthcare, there is a tendency to attempt to provide in-home assisted living to elderly people, staying alone, by making use of human activity monitoring. This application is of a major importance for the ageing population, and would increase the safety of aged people by, e.g., detecting falls, preventing disease, and identifying disability. In short, the above mentioned potential healthcare applications are enough to underline the significance of developing human activity monitoring systems. At the heart of such a system design and implementation,

The associate editor coordinating the review of this manuscript and approving it for publication was Hayder Al-Hraishawi.

the time-variant (TV) velocity of motion (TV speed and TV angle of motion (AOM)) has particularly been adopted as a potential metric from which information on a user's behavior can be extracted and identified. Current approaches to velocity estimation are computer vision, on-body sensing, and radio frequency (RF) signal analysis [2]. In computer vision-based approaches, the TV velocity of a walking person is extracted by analysing continuously recorded video. In the case of on-body sensing, velocity estimation can be achieved by using sensors, such as accelerometers and gyroscopes, attached to different parts of a person's body or deployed in the indoor space. Finally, the last approach relies on using rooms equipped with radars or simple wireless communication systems. In this case, the modification induced by a person's motion on the Doppler characteristics of the propagating radio signal is exploited to obtain the velocity.

Within the context of ADLs tracking techniques, this method is sometimes referred to as device-free ADL, and is attracting a lot of attention over the past few years due to its high potential in providing an accurate estimate of the TV velocity (TV speed and TV AOM) of moving persons. The topic of this article falls within the scope of TV velocity or speed estimation using RF-based approaches. Specifically, we present an accurate iterative procedure to estimate the velocity of a single moving person in two-dimensional (2D) indoor environments by using RF techniques. We consider a distributed 2×2 multiple-input multiple-output (MIMO) system, and a scenario where the velocity is TV and the propagation environment is non-stationary.

It is worthwhile at this point to mention that, aside from ADLs tracking applications, speed estimation of mobile units has intensively been studied within the context of mobile radio communications. In fact, speed estimation is prevalent in mobile radio communications, while TV velocity determination is of relevance in human activity recognition. In the following, we provide a literature review regarding each of these topics independently. For convenience, the available methods along with the contribution of the paper are summarized in Fig. 1.

A. RELATED WORKS

This section presents a review of existing techniques to estimate the TV velocity/speed of moving objects/persons. To do so, we will start by discussing (constant) speed estimation procedures in the context of mobile radio communications. Then, we will review TV velocity estimation techniques for indoor ADLs tracking. In the following, we distinguish between the terms velocity and speed. The term ''velocity'' is a vector, the magnitude of which indicates the speed, while the AOM describes the direction.

1) SPEED ESTIMATION TECHNIQUES IN MOBILE RADIO COMMUNICATIONS

Mobile speed determination has a rich history in wireless communications. Estimation techniques have been proposed in the context of handover algorithm design to ensure reliable mobile radio communications for both micro-cellular and multitier systems, e.g., by significantly reducing the probability of dropped calls [3]. Reliable mobile station (MS) speed estimates improve the receiver performance through more effective dynamic channel allocation and optimization of adaptive multi-access radio receivers [3], [4]. Since the performance of receiving techniques is highly dependent on the distortion caused by the mobile radio channel, the Doppler frequency, or equivalently, the MS's speed, plays a key role in controlling the receiver parameters.

The estimation of the speed of mobile units can be performed by exploiting the statistical properties of numerous features of the received signal such as its envelope and phase. In this context and as summarized in Fig. 1, three major classes of speed estimation techniques were presented in the literature: crossing-and covariance-based approaches, maximum likelihood-based (ML) methods, and power spectrum-based procedures. Crossing-based approaches calculate the number of level-crossings of the channel envelope or phase which is proportional to the MS's speed. For example, the adaptive hand-off algorithms for microcellular systems in [28] use level-crossing rate (LCR)-based velocity estimation methods for Rice fading. In [5], speed estimation procedures were presented based on the in-phase component zero-crossing rate, in-phase component rate of maxima, and LCR using diversity combining techniques in Rayleigh flat fading channels. Later, the authors of [6] investigated the robustness against noise of an iterative Doppler shift estimator utilizing the LCR of the channel envelope. On the other hand, covariance-based algorithms determine the maximum Doppler frequency by means of the autocovariance of the received signal. The technique of covariance-based MS speed estimation was first considered in [7] and subsequently in [8], where the MS's speed was estimated using the auto-covariance of the channel power gain of the received signal. A generalization of this work using the integral-power sum of the in-phase and quadrature components of the complex channel gain and the integral powers of the channel envelope was reported in [9]. An adaptive averaging methodology for handoffs in cellular systems using covariance-based speed estimation was proposed in [10] assuming Rayleigh and Rice fading channels. Also, a speed estimator based on the spectral moments and the correlation properties of the in-phase and the quadrature components as well as the envelope of the received signal was developed in [11] assuming isotropic scattering conditions. It should be mentioned that the aforementioned techniques assume and are limited to isotropic scattering conditions. For the case of wide-sense stationary (WSS) fading channels under non-isotropic fading conditions, a parametric Doppler spread estimation procedure was been reported in [12] based on the auto-correlation properties of the complex channel gain. Among the existing speed estimation techniques, cross- and covariance-based approaches were extensively studied in the literature for numerous fading channel models, due to their low complexity. To the best of the authors' knowledge, there are no results regarding the

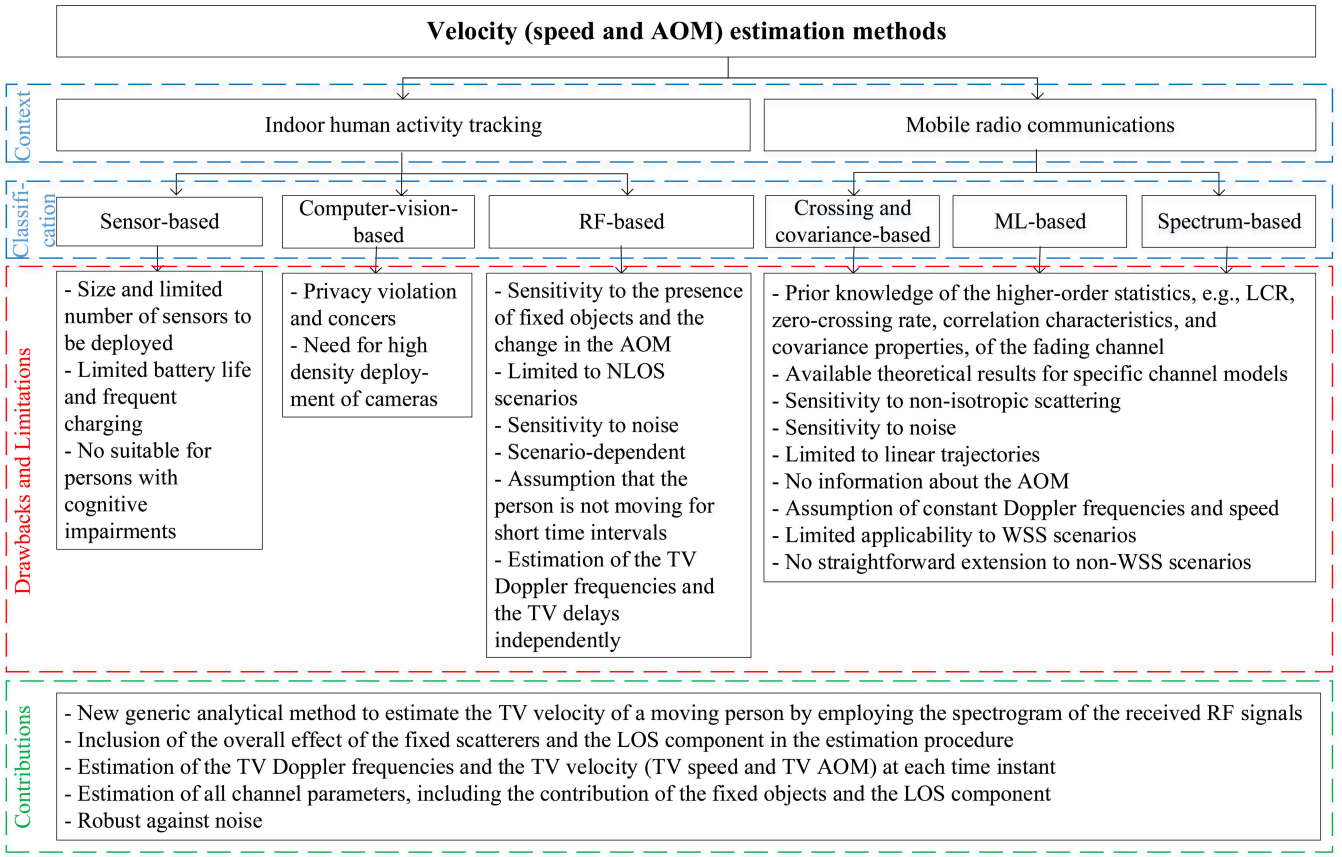

FIGURE 1. Classification of existing TV velocity/speed estimation methods, limitations, and contributions.

higher-order statistical properties of non-stationary channels under non-isotropic scattering conditions. Apart from the crossing and covariance based methods, speed estimation was as well approached by applying the ML method. Although they are near-optimal, ML-based methods are very complex to implement. They require the knowledge of the signal-to-noise ratio (SNR) and were shown to be very sensitive to noise [13], [14]. An example of an ML-based algorithm relying on a periodic channel estimation was derived in [14]. In addition, the effects of non-isotropic scattering conditions and the presence of a line-of-sight (LOS) component on the performance of ML-based speed estimators were investigated in [14] and [15]. Later, new estimation methods were introduced [16]–[18] utilizing the power spectrum of the received signals. Speed estimation algorithms based on the integration or differentiation of the power spectrum density of mobile fading channels were reported in [16] and [17]. The authors of [18] proposed a non-parametric speed estimation algorithm by exploiting the properties of the power spectrum of mobile fading channels, which is not only robust against noise but also insensitive to non-isotropic scattering conditions.

It should be noted that, although the estimation techniques developed in the context of mobile radio communications provide an accurate estimation of the speed of the mobile units, their applicability is limited to scenarios where the MSs are moving along a straight line and with constant speed (WSS fading channels). Furthermore, it should be stressed that these methods only estimate the (constant) speed of the mobile units while ignoring all information about their trajectory, i.e., AOM. For non-stationary scenarios, the majority of the estimation techniques were developed in the context of velocity-based ADL tracking. An overview of these methods will the topic of the next part of the introduction.

2) VELOCITY ESTIMATION-BASED HUMAN ACTIVITY MONITORING TECHNIQUES

As can be seen on the left-hand side of Fig. 1, in the context of indoor human activity tracking, the available approaches for TV velocity estimation can, roughly, be grouped into three classes: sensor (device)-based, computer-vision-based, and RF-based approaches.

Early studies on ADL tracking were developed using the vision method. The basic components of this technique are cameras recording of motion and robust image processing techniques for acitivity recognition. Here, the speed of a walking person is extracted by analysing continuously recorded video [19]–[22]. For example, the authors of [19] employed the Microsoft Kinect (camera device), which was primarily developed in the context of controller free gaming, to acquire spatial and temporal gait parameters for in-home

fall risk assessment. Moreover, a red, green, and blue (RGB)-depth camera-based ADL recognition technique was presented in [20], focusing on fall related activities such as falling from a sitting position, falling from standing, and falling from a standing position. Another video-based method for tracking as well as recognizing moving objects in indoor areas using a Markovian model was reported in [21]. A major criticism of this method is that it violates privacy. In addition, the method requires good lightning, high-density deployment of cameras, and great computer power.

In recent years, motivated by the rapid progress of sensors technology and the internet-of-things, activity monitoring moved toward the application of sensor-based approaches. In these methods, sensors are attached to different parts of a person's body or deployed in indoor environments. Studies have shown that this approach is not appropriate, and is not the right choice, especially, for older people [23]–[28]. Non-wearable sensor systems, e.g., laser rangefinders and infrared sensors, are usually placed along the floor on the ''force platform'', where the gait velocity information is extracted by means of pressure sensors and/or ground reaction sensors [23], [24]. In this situation, it should be pointed out that the sensors need a controlled environment and the person is supposed to walk along a predefined trajectory. Another solution, for avoiding body-worn sensors, consists on planting the sensors on clothing items of the person. In wearable sensor-based systems, such as accelerometers, gyroscopes, magnetometers, and ''push buttons'', instead, the sensors can be planted on the clothing items or attached to human body segments, e.g., head, knees, feet, hands, thighs or waist [25]. Typical examples describing the implementation of this technique can be found in [28]. The Run3D gait velocity analysis device is an on-body sensing system, reported in [27], is an example of on-body sensing system with a 3-axis accelerometer, magnetometer, and gyroscope, which are located on the lower back (pelvis and hip) and along the lower limbs (knees and ankles) of a person. In summary, the employability of the sensor-based method is unfortunately limited by the constrained size number of sensors and the battery life and charge, especially for patients with cognitive impairments.

Along with the vision-based and sensor-based approaches, profiting from the potentials of modern wireless communication systems and to overcome the aforementioned limitations, RF-based ADLs monitoring has become a hot topic of research in recent years. In this third approach, TV velocity estimation is accomplished by exploiting the fading characteristics of RF signals of an in-home radio system. This method is, obviously, suitable for overcoming the aforementioned limitations. Namely, it is used to estimate the TV velocity of persons without equipping them with devices (sensors), which in turn allows them to perform in-home ADLs in a natural way [29]–[32]. In particular, such a technology explores the way the human motion affects the radio signals of in-home wall/floor-mounted transceivers to extract the TV velocity of a walking person. The WiGait system is an example of such systems developed for determining the gait velocity [29]. Another interesting speed-based indoor localization work can be found in [30], where channel state information (CSI) data is used in conjunction with Wi-Fi. The authors of [31] proposed the Emerald product. This system monitors the three-dimensional (3D) motion of persons through the analysis of the TV phase of the complex channel gain of the RF signal. Moreover, the RF-Capture system for RF-based ADLs tracking was developed in [32]. This system captures the figure of a person when it is in complete darkness. One of the drawback of the studies reported in [30]–[33] is that their accuracy is greatly influenced by the rich multipath structure exhibited by non-stationary indoor channels. Recently, with the growing interest in the millimeter wave (mmWave) technology, the mmVital system was introduced in [33] to track and follow the breathing and heart rate of persons in indoor areas. This task is achieved by transmitting 60 GHz mmWave signals and analysing the strength of the received signal. Additionally, in-home radar monitoring devices have been introduced as a potential leading technology for future activity tracking systems in indoor environments [34]–[36]. The interest in investigating radar-based techniques comes from their proven technology, privacy preservation, and safety. Radar systems are based on the analysis of the propagation delays and Doppler frequencies of the received signal. The Doppler signatures are obtained by observing the TV phase of the received signal which provides insight into the main features that describe and classify human motions. The dynamic nature of fall signals was investigated in, e.g., [34], using the mel-frequency[1] cepstral coefficients. In [35], the wavelet transform was applied to the analysis of radar fall signals and the extraction of fall features. Later, the velocity-based decimeter-level tracking device Widar1.0 was proposed in [37] and further developed in [38] to Widar2.0, an indoor submeter tracking system. In addition, the performance of Widar2.0 was compared with that of existing estimation methods such as the dynamic-MUSIC [39] and IndoTrack [40] and the results show that Widar2.0 offers the best estimation accuracy. However, it is worth pointing out that the approach in [38] estimates TV Doppler frequencies and TV delays independently from each other without considering the relationship between these quantities. Furthermore, it should be mentioned that several Wi-Fi-based in-home monitoring systems with a submeter accuracy have been developed [41]–[43]. However, these systems only operate in non-line-of-sight (NLOS) scenarios and require the moving person to carry a wireless device (phone, bracelet, etc.). In this area of applications, and as summarized in Fig. 1, the available approaches for TV velocity estimation can face several challenges such as a high false activity classification rate, occlusion between the transmitter and the receiver, sensitivity to fixed scatterers caused by the furniture

[1]The abbreviation ''mel'' comes from the signal melody to indicate that the scale is based on pitch comparisons. It is commonly used as a short-term representation of a sound in speech recognition systems.

and the interior walls as well as the direction of motion of the moving objects (persons, pets) with respect to the radar LOS component, and the presence of multiple moving objects in the indoor environment.

3) LIMITATIONS OF EXISTING TECHNIQUES AND MOTIVATION

The interest in accurate speed or velocity estimation has increased significantly in recent decades to track the motion of objects/persons in indoor and outdoor environments. As described above and summarized in Fig. 1 (red box), it can be concluded that existing speed estimation techniques suffer from one or more of the following limiting assumptions that the person does not move for a period of time or moves at constant speed or on a linear trajectory. Other drawbacks and limitations may include: a propagation under isotropic scattering, a high sensitivity to the rich scattering structure (resulting from the furniture) of indoor environments, dependency on the presence or absence of the LOS component, and that no information regarding the AOM is available, etc. Therefore, there exist, to date, no generalized method that allows the estimation of the TV velocity, i.e., TV speed and TV AOM, of moving persons in non-stationary indoor environments for a given time instant. Motivated by these facts, our main objective in this work is to contribute to the topic of velocity/speed-based tracking and monitoring of ADL by proposing a new iterative method to evaluate the TV speed and TV AOM of a moving person in indoor spaces. The method, which is robust against noise, takes into account both fixed and moving objects.

B. CONTRIBUTIONS

In this work, we propose a new accurate and noise-robust RF-based method to estimate the TV velocity (TV speed and TV AOM), of a single moving person in an indoor area, considering the effects of the moving scatterer, the fixed scatterers, and the LOS component. The estimation procedures developed in this article are inspired by the iterative non-linear least square approximation (INLSA) algorithm initially, which was proposed in [44]. Later, this method was further investigated to design measurement-based wideband channel simulators by using the time-frequency correlation function [45] and TV channel impulse response [46], [47]. Unfortunately, it can only be applied to WSS multipath fading channels, i.e., scenarios where the speed of the moving person is assumed to be constant and the trajectory is linear. Namely, it cannot be readily exploited to estimate velocity of moving person in non-stationary channels due to the main fact that the relation of proportionality between the speed and maximum Doppler frequency does not hold. This article aims to pave the way for a theoretical study in which the conventional INSLA approach [44] is extended to deal with RF-based estimation of the TV velocity of a moving person in non-stationary propagation environments.

To do so, we start by modelling the indoor propagation phenomenon according to the two-dimensional (2D) fixed-to-fixed non-stationary channel model introduced in [48]. For simplicity, the walking person is described by a single moving point scatterer, which reflects one of the person's body parts such as the head, the center of gravity, the waist etc. The fixed (stationary) scatterers reflect the fixed objects in the indoor area, e.g., walls, windows, furniture (chairs, tables, etc.) and decoration items (books, frames, shelves, etc.). The room is be equipped with a distributed 2×2 MIMO system, which consists of two antenna elements on both the transmitter and the receiver sides. The concept of the estimation procedure proposed in this article was initially introduced in [1] for a single moving person using mmWave signals. Similar results were introduced for three-dimensional indoor environments and multiple moving persons in indoor areas in [49] and [50], respectively. In this article, we extend the work in [1] to the case of general carrier frequencies and simplify the analytical steps leading to solving the underlying optimization problems.

The proposed algorithm is divided into two major parts. In the first part, the path gains, initial phases of the channel, and TV Doppler frequencies are estimated by fitting the spectrograms of the channel model in [48] to the spectrograms of the received signals. Closed-form expressions are derived for the estimates of the path gains of the moving scatterer (person) and overall fixed scatterers as well as the initial phase of the channel and the TV Doppler frequencies, which reduces the initial five-dimensional estimation problem to a 2D optimization problem. In the second part of our algorithm, the estimated instantaneous Doppler frequencies are utilized to estimate the TV velocity, i.e., TV speed and TV AOM, of the moving person as well as the TV angles-of-departure (AODs) and TV angles-of-arrival (AOAs). Here, exact closed-form expressions are derived for the new estimates of the TV speed, TV AODs, and TV AOAs, leading to a one-dimensional optimization problem. In both algorithms, the computation of the channel parameters relies on the minimization of the Euclidean norm of the introduced fitting errors. The validity of the proposed procedure has been verified by comparing the obtained estimated parameters of interest, i.e., TV Doppler frequencies and TV speed, with computer-simulated test signals. The effects of noise on the estimation accuracy of the proposed procedure have been investigated and numerical results show that the presented estimation method is robust against noise.

The main contributions of this article are summarized as follows.

- The proposed iterative method employs the spectrogram of the complex channel gain of the received RF signal to estimate the instantaneous velocity of a moving person (modelled by a single point scatterer) in indoor areas which are equipped with a distributed 2×2 MIMO system.
- The overall effect of the fixed scatterers (objects) and the LOS component are included in the optimization problem.

- The technique is based on the minimization of the Euclidean norm of the fitting error and is divided into two parts. First, we estimate the TV Doppler frequencies by fitting the spectrogram of the channel model to the spectrogram of the RF signal. Then, the corresponding TV velocity, i.e., TV speed and TV AOM, is deduced by matching the Doppler frequencies of the channel model to those previously estimated.
- Together with the determination of the TV velocity, this method estimates all channel parameters, including the path gain of the moving scatterer, the path gain of the overall fixed scatterers, the AOAs, and the AOD.
- Exact and approximate closed-form expressions to the estimates of the channel parameters are derived which considerably reduced the computational complexity of the underlying optimization problems.
- The utilization of the spectrogram reduces the impact of noise on the accuracy of the estimation. In fact, the spectrogram is computed by as the squared short-time Fourier transform, which is obtained by averaging the complex channel gain for short intervals of the running time.
- Finally, computer simulations are presented to validate the accuracy and robustness against noise of the presented algorithm for several speed models.

The remainder of this article is structured as follows. Preliminaries and useful background material are presented in Section II. Section III describes the proposed two-parts iterative procedure to estimate the TV velocity of a moving person. Numerical results are discussed in Section IV. Finally, Section V outlines the conclusions.

II. PRELIMINARIES AND BACKGROUND MATERIAL

In this section, we first provide a description of the geometrical indoor propagation scenario assumed in this study. The spectrogram of the resulting RF signal is then given together with the corresponding TV Doppler shift.

A. ROOM LAYOUT AND PROBLEM DESCRIPTION

The objective of this article is to present a novel and robust estimator of the TV velocity, i.e., speed and AOM, of a walking person based on the analysis of RF signals of a 2×2 MIMO system. Fig. 2 shows a typical living room, with the walking person, the distributed transmit antennas A_1^T and A_2^T, and receive antennas A_1^R and A_2^R of the MIMO system. The geometry of the corresponding 2D indoor multipath propagation model is depicted in Fig. 3. In this setting, we consider a room with length A and width B centralized at the origin O. The antennas A_1^T and A_2^T (A_1^R and A_2^R) are located at the fixed positions (x_1^T, y_1^T) and (x_2^T, y_2^T) ((x_1^R, y_1^R) and (x_2^R, y_2^R)), respectively. Also, there is only one person moving in the room. For simplicity, this person is modelled by a single moving scatterer S^M, which represents its center of gravity, located at the initial position (x^M, y^M). The trajectory of the moving person is described by TV speed

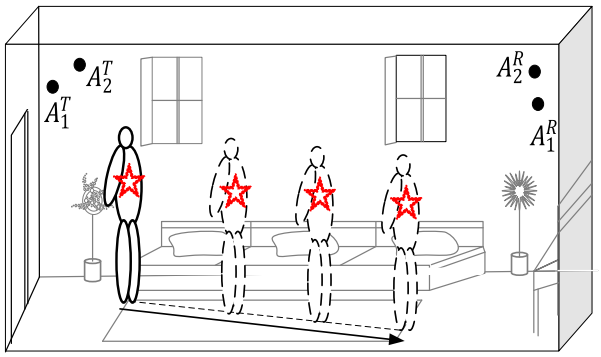

FIGURE 2. Indoor space architecture with 4 distributed antennas (A_1^T, A_2^T, A_1^R, and A_2^R), stationary objects (walls, objects ...), and the walking person [1].

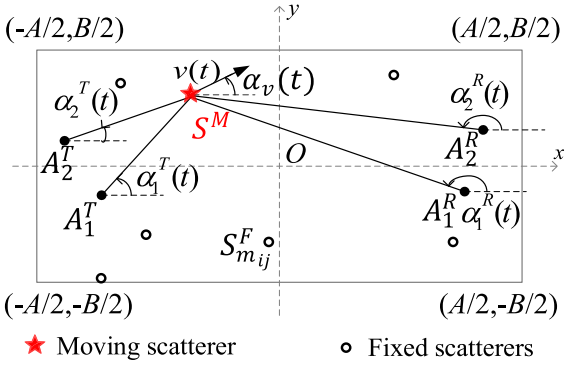

FIGURE 3. Geometrical model of a 2×2 MIMO indoor channel with a moving scatterer S^M (walking person) [1].

$v(t)$ and TV AOM $\alpha_v(t)$. The TV displacements $x(t)$ and $y(t)$ along the x-and y-axis of the person (scatterer S^M) can be expressed as $x(t) = x^M + \int_0^t v(u)\cos(\alpha_v(u))du$ and $y(t) = y^M + \int_0^t v(u)\sin(\alpha_v(u))du$, respectively. Moreover, the scenario includes walls and fixed objects which are modelled by M_{ij} fixed scatterers $S_{m_{ij}}^F$ ($m = 1, 2, .., M_{ij}$), seen between the transmit antenna A_j^T and receive antenna A_i^R. Furthermore, single-(multiple-)bounce scattering is considered for the moving scatterer (fixed scatterers).

B. SPECTROGRAM

In this secction, we review the spectrogram of the complex channel gain of the propagation scenario introduced in Section II.A and present some useful preliminary results. Assuming perfect CSI at the receiver side, the complex channel gain $\mu_{ij}(t)$ between the jth transmit antenna and ith receive antenna $(i, j = 1, 2)$ is given by [48]

$$\mu_{ij}(t) = c_{ij}\exp\left[j\theta_{ij}(t)\right] + \sum_{m_{ij}=1}^{M_{ij}} c_{m_{ij}}\exp\left(j\theta_{m_{ij}}\right) \qquad (1)$$

where the first single term refers to the component resulting from the moving scatterer S^M and the second term represents the multipath components coming from the M_{ij} fixed

scatterers $S^F_{m_{ij}}$, $m_{ij} = 1, 2, .., M_{ij}$. Here, the quantity c_{ij} ($c_{m_{ij}}$) refers to the path gain of the moving (m_{ij}th fixed) scatterer. The TV channel phase $\theta_{ij}(t)$ is expressed in terms of the TV Doppler frequency $f_{ij}(t)$ as $\theta_{ij}(t) = 2\pi \int_0^t f_{ij}(x)dx + \theta_{0,ij}$ [48], where $\theta_{0,ij}$ is the initial channel phase, which is modelled as a random variable with a uniform distribution over the interval $[0, 2\pi)$. The TV Doppler frequency $f_{ij}(t)$ can be expressed as

$$f_{ij}(t) = -f_{\max}(t)\left[\cos\left(\alpha_j^T(t) - \alpha_v(t)\right) + \cos\left(\alpha_i^R(t) - \alpha_v(t)\right)\right] \tag{2}$$

in which $f_{\max}(t) = f_0 v(t)/c_0$ denotes the TV maximum Doppler frequency, with f_0 and c_0 being the carrier frequency and the speed of light, respectively. In (2), $\alpha_j^T(t)$ ($\alpha_i^R(t)$) stands for the AOD (AOA) corresponding to the jth (ith) transmit (receive) antenna, which is given by $\alpha_j^T(t) = \arcsin[(y(t) - y_j^T)/(x(t) - x_j^T)]$ ($\alpha_i^R(t) = \arcsin[(y(t) - y_i^R)/(x(t) - x_i^R)]$). In (1), the phases $\theta_{m_{ij}}$ are assumed to be independent and identically distributed random variables, uniformly distributed over the interval $(0, 2\pi]$. For brevity, the sum $\sum_{m_{ij}=1}^{M_{ij}} c_{m_{ij}} \exp\left(j\theta_{m_{ij}}\right)$ in (1) will be replaced by a single complex random variable term $n_{M_{ij}} = C_{F_{ij}} \exp(j\vartheta_{F_{ij}})$, where $C_{F_{ij}} = \sqrt{(\sum_{m_{ij}=1}^{M_{ij}} c_{m_{ij}} \cos(\theta_{m_{ij}}))^2 + (\sum_{m_{ij}=1}^{M_{ij}} c_{m_{ij}} \sin(\theta_{m_{ij}}))^2}$ and $\vartheta_{F_{ij}} = \text{atan2}(\sum_{m_{ij}=1}^{M_{ij}} c_{m_{ij}} \sin(\theta_{m_{ij}}), \sum_{m_{ij}=1}^{M} c_{m_{ij}} \cos(\theta_{m_{ij}}))$. Here, the the multi-valued inverse tangent function atan2 function is employed because it returns a single correct and unambiguous value for the phase in the interval $(-\pi, \pi]$ of a complex number written in polar coordinates.

For the determination of closed-form solutions to the new estimates of the channel parameters, we review some key characteristics of non-stationary channels. We shall start by alternatively writing the TV complex channel gain $\mu_{ij}(t)$ in (1) as $\mu_{ij}(t) = R_{ij}(t)\exp(j\phi_{ij}(t))$, where $R_{ij}(t)$ and $\phi_{ij}(t)$ are the channel envelope and phase, respectively. The channel envelope $R_{ij}(t) = |\mu_{ij}(t)|$ is given by

$$R_{ij}(t) = \sqrt{c_{ij}^2 + C_{F_{ij}}^2 + 2c_{ij}C_{F_{ij}} \cos\left(\theta_{ij}(t) - \vartheta_{F_{ij}}\right)}. \tag{3}$$

The expression of the channel phase $\phi_{ij}(t)$ is given by $\phi_{ij}(t) = \text{atan2}[c_{ij}\sin(\theta_{ij}(t)) + C_{F_{ij}}\sin(\vartheta_{F_{ij}}), c_{ij}\cos(\theta_{ij}(t)) + C_{F_{ij}}\cos(\vartheta_{F_{ij}})]$.

For short time intervals in which the Doppler frequencies $f_{ij}(t)$ can be approximated by linear functions (a first-order Tayler series expansion), the spectrogram $S_{ij}(f, t)$ of $\mu_{ij}(t)$ in (1) is expressed as [48]

$$S_{ij}(f, t) = S_{ij}^{(a)}(f, t) + S_{ij}^{(c)}(f, t) \tag{4}$$

where the auto-term $S_{ij}^{(a)}(f, t)$ is given by

$$S_{ij}^{(a)}(f, t) = c_{ij}^2 G\left(f, f_{ij}(t), \sigma_{1,ij}^2\right) + G\left(f, 0, \frac{\sigma_0^2}{2}\right) C_{F_{ij}}^2 \tag{5}$$

in which $G(a, b, c) = \exp[-(a-b)^2/(2c)]/(\sqrt{2\pi c})$, $\sigma_0^2 = 1/(2\pi\sigma_w)^2$, and $\sigma_{1,ij}^2 = (\sigma_0^2 + \sigma_w^2 k_{ij}^2)/2$, with k_{ij} being defined according to [48, Eq. (40)] and σ_w^2 denoting the spread of the Gaussian window utilized in the short-time Fourier transformation leading to the derivation of the spectrogram. The expression of the cross-term $S_{ij}^{(c)}(f, t)$ is given by [48, Eq. (35)].

$$S_{ij}^{(c)}(f, t) = \frac{2c_{ij}C_{F_{ij}}}{\sigma_w\sqrt{\pi}} \Re\left\{G\left(f, f_{ij}(t), \sigma_{2,ij}^2\right) G^*\left(f, 0, \sigma_0^2\right) \cdot \exp\left(j\left(\theta_{ij}(t) - \vartheta_{F_{ij}}\right)\right)\right\} \tag{6}$$

where $\sigma_{2,ij}^2 = \sigma_0^2 - jk_{ij}/(2\pi)$.

It is worth pointing out that for the general case, the Doppler frequencies in (2) cannot be represented by linear functions. However, to ensure that this linearity assumption stands valid, the total observation time is divided into subintervals of duration T_0, with $T_0 < \sigma_w$. During the period T_0, the instantaneous Doppler frequencies $f_{ij}(t)$ can be approximated by a linear function, which is characterized by its slope k_{ij}. The parameter k_{ij} is updated from one sub-interval to the next. Hence, the slope k_{ij} is TV for the total observation time and will be denoted by $k_{ij}(t)$.

As is detailed in the Appendix, the product of Gaussian functions $G\left(f, f_{ij}(t), \sigma_{2,ij}^2\right) G^*\left(f, 0, \sigma_0^2\right)$ in (6) can be further simplified. Thus, by substituting (38) in (6), the cross-term $S_{ij}^{(c)}(f, t)$ can alternatively be expressed as

$$S_{ij}^{(c)}(f, t) = \frac{2c_{ij}C_{F_{ij}}}{\sigma_w\pi\sqrt{2}} \Re\left\{\frac{g_{ij}(t)}{\sigma_{3,ij}} \exp\left(-\frac{\left(f - m_{ij}(t)\right)^2}{2\sigma_{3,ij}^2}\right) \cdot \exp\left(j\left(\theta_{ij}(t) - \vartheta_{F_{ij}}\right)\right)\right\} \tag{7}$$

where $g_{ij}(t)$ is given in (38), $m_{ij}(t) = \sigma_0^2 f_{ij}(t)/(\sigma_{2,ij}^2 + \sigma_0^2)$, and $\sigma_{3,ij}^2 = \sigma_{2,ij}^2\sigma_0^2/(\sigma_{2,ij}^2 + \sigma_0^2)$. Profiting from the facts that $\sigma_w \ll 1$ and σ_w is inversely proportional to k_{ij}, the function $g_{ij}(t)$ can be further simplified and be approximated as in (39). In turn, it can be shown that the cross-term $S_{ij}^{(c)}(f, t)$ can be approximated by

$$S_{ij}^{(c)}(f, t) \approx \frac{c_{ij}C_{F_{ij}}}{\pi^{\frac{3}{2}}\sigma_w} \Re\left\{\frac{1}{\sigma_{3,ij}\sqrt{\sigma_{2,ij}^2 + \sigma_0^2}} \exp\left(-\frac{\left(f - m_{ij}(t)\right)^2}{2\sigma_{3,ij}^2}\right) \cdot \exp\left(j\left(\theta_{ij}(t) - \vartheta_{F_{ij}}\right)\right)\right\}. \tag{8}$$

Moreover, the TV Doppler shift $B_{\mu_{ij}}^{(1)}(t)$ can be obtained in terms of the spectrogram $S_{ij}(f, t)$ as $B_{\mu_{ij}}^{(1)}(t) = \int_{-\infty}^{\infty} f S_{ij}(f, t)df \,/\, \int_{-\infty}^{\infty} S_{ij}(f, t)df$ [48]. Employing (5) and (7), and then integrating with respect to the variable f yield the following exact expression for the TV Doppler shift $B_{\mu_{ij}}^{(1)}(t)$

$$B_{\mu_{ij}}^{(1)}(t) = \frac{c_{ij}^2 f_{ij}(t) + \frac{2c_{ij}C_{F_{ij}}\Re\left\{g_{ij}(t)m_{ij}(t)\exp\left(j\left(\theta_{ij}(t) - \vartheta_{F_{ij}}\right)\right)\right\}}{\sigma_w\sqrt{\pi}}}{c_{ij}^2 + C_{F_{ij}}^2 + \frac{2c_{ij}C_{F_{ij}}\Re\left\{g_{ij}(t)\exp\left(j\left(\theta_{ij}(t) - \vartheta_{F_{ij}}\right)\right)\right\}}{\sigma_w\sqrt{\pi}}}. \tag{9}$$

Furthermore, by utilizing (8), a closed-form approximate solution to the exact expression of the TV Doppler shift

$B_{\mu_{ij}}^{(1)}(t)$ in (9) can be obtained as

$$B_{\mu_{ij}}^{(1)}(t) \approx \frac{c_{ij}^2 f_{ij}(t) + \frac{\sqrt{2}c_{ij}C_{F_{ij}}}{\sigma_w \pi} \Re\left\{ \frac{m_{ij}(t) \exp\left(j\left(\theta_{ij}(t) - \vartheta_{F_{ij}}\right)\right)}{\sqrt{\sigma_{2,ij}^2 + \sigma_0^2}} \right\}}{c_{ij}^2 + C_{F_{ij}}^2 + \frac{\sqrt{2}c_{ij}C_{F_{ij}}}{\sigma_w \pi} \Re\left\{ \frac{\exp\left(j\left(\theta_{ij}(t) - \vartheta_{F_{ij}}\right)\right)}{\sqrt{\sigma_{2,ij}^2 + \sigma_0^2}} \right\}}. \quad (10)$$

Equations (9) and (10) will be utilized in the next section to compute closed-form solutions to the gain of the overall fixed scatterers $C_{F_{ij}}$ and the TV Doppler frequency $f_{ij}(t)$. The description of the proposed estimation procedures will be the topic of the following section.

III. ESTIMATION OF THE TIME-VARIANT VELOCITY OF A MOVING PERSON

This section describes the different steps of the proposed the two-parts estimation method to determine the TV velocity parameters of a moving person in an indoor area, where the propagation scenario is modelled as detailed in Section II. For this purpose, we will first estimate the TV Doppler frequencies.

A. ESTIMATION OF THE TIME-VARIANT DOPPLER FREQUENCIES

In practice, the received RF signal, which is observed during a time interval $[0, T]$ and in the frequency bandwidth $[-B/2, B/2]$, is in the form of samples at discrete frequencies $f_q = -B/2 + q\Delta f \in [-B/2, B/2]$, $q = 0, .., Q-1$ and discrete time instances $t_p = p\Delta t \in [0, T]$, $p = 0, .., P-1$. Here, Δf and Δt are the frequency and time sampling periods, respectively. The spectrogram of the simulated channel is computed from the samples of the received radio signal. Thus, the spectrogram is obtained as samples in both time and frequency domains.

Let us denote by $\hat{\mu}_{ij}(t_p)$ the complex channel gain of the received RF signal and $\hat{S}(f_q, t_p)$ the corresponding spectrogram, which is obtained by the procedure reported in [48]. The problem at hand is to determine a set of parameters $\mathcal{P}_1(t_p) = \{\tilde{c}_{ij}, \tilde{k}_{ij,p}, \tilde{f}_{ij,p}, \tilde{\theta}_{0,ij}, \tilde{C}_{F_{ij}}, \tilde{\vartheta}_{F_{ij}}\}$, where the quantities $\tilde{c}_{ij}$, $\tilde{f}_{ij,p}$, $\tilde{\theta}_{0,ij}$, $\tilde{C}_{F_{ij}}$, and $\tilde{\vartheta}_{F_{ij}}$ refer to the estimated values of c_{ij}, $f_{ij,p} = f_{ij}(t_p)$, $\theta_{0,ij}$, $C_{F_{ij}}$, and $\vartheta_{F_{ij}}$, respectively. The computation of the channel parameters is performed in such a way that the spectrogram $\tilde{S}_{ij}(f_q, t_p)$ of the channel model matches the spectrogram $\hat{S}_{ij}(f_q, t_p)$ of the received RF signal. Here, $\tilde{S}_{ij}(f_q, t_p)$ refers to the spectrogram of the complex channel gain $\tilde{\mu}(t_p)$ of the channel model sampled in both time and frequency. The expression of the spectrogram $\tilde{S}_{ij}(f_q, t_p)$ is obtained according to (1) by replacing $c_{ij}, f_{ij,p} = f_{ij}(t_p)$, $\theta_{0,ij}$, $C_{F_{ij}}$, and $\vartheta_{F_{ij}}$ by $\tilde{c}_{ij}, \tilde{f}_{ij,p}, \tilde{\theta}_{0,ij}, \tilde{C}_{F_{ij}}$, and $\tilde{\vartheta}_{F_{ij}}$, respectively. For this purpose, we start by introducing the object function for determining the set $\mathcal{P}_1(t_p)$ as

$$E_1\left(\mathcal{P}_1(t_p)\right) = \left|\left|\hat{S}_{ij}(f_q, t_p) - \tilde{S}_{ij}(f_q, t_p)\right|\right|_2^2. \quad (11)$$

By replacing the spectrogram $\tilde{S}_{ij}(f_q, t_p)$ with its expression obtained from (4)−(7), the object function in (11) can be alternatively written as

$$\begin{aligned} E_1\left(\mathcal{P}_1(t_p)\right) &= \left|\left|\hat{\mathbf{s}}_{ij,p} - \tilde{c}_{ij}^2 G\left(f_q, \tilde{f}_{ij,p}, \tilde{\sigma}_{1,ij,p}^2\right) - G\left(f_q, 0, \frac{\sigma_0^2}{2}\right)\tilde{C}_{F_{ij}}^2 \right.\right. \\ &\quad - \frac{2\tilde{c}_{ij}\tilde{C}_{F_{ij}}}{\sigma_w\sqrt{\pi}} \Re\left\{ \frac{\exp\left(j\left(\tilde{\theta}_{ij,p} - \tilde{\vartheta}_{F_{ij}}\right)\right)}{\tilde{g}_{ij,p}^{-1}\tilde{\sigma}_{3,ij,p}\sqrt{2\pi}} \right. \\ &\quad \left.\left. \exp\left(-\frac{\left(f_q - \tilde{m}_{ij,p}\right)^2}{2\tilde{\sigma}_{3,ij,p}^2}\right)\right\}\right|\Big|_2^2 \end{aligned} \quad (12)$$

where $\hat{\mathbf{s}}_{ij,p}$ is a column vector containing the stacked values of $\hat{S}_{ij}(f_q, t_p)$ for increasing values of q. Here, $\tilde{\sigma}_{1,ij,p}^2 = (\sigma_0^2 + \sigma_w^2\tilde{k}_{ij,p}^2)/2$, $\tilde{\sigma}_{2,ij,p}^2 = \sigma_0^2 - j\tilde{k}_{ij,p}/(2\pi)$, and $\tilde{\sigma}_{3,ij,p}^2 = \tilde{\sigma}_{2,ij,p}^2\sigma_0^2/(\tilde{\sigma}_{2,ij,p}^2 + \sigma_0^2)$, in which $\tilde{k}_{ij,p}$ is the estimated value of $k_{ij,p} = k_{ij}(t_p)$. In (12), the quantities $\tilde{\theta}_{ij,p}$, $\tilde{g}_{ij,p}$ and $\tilde{m}_{ij,p}$ are given by $\tilde{\theta}_{ij,p} = 2\pi\int_0^{t_p}\tilde{f}_{ij}(u_p)du_p + \tilde{\theta}_{0,ij}$, $\tilde{g}_{ij,p} = \exp(-\tilde{f}_{ij,p}^2/[2(\tilde{\sigma}_{2,ij,p}^2 + \sigma_0^2)])/\sqrt{2\pi(\tilde{\sigma}_{2,ij,p}^2 + \sigma_0^2)}$, and $\tilde{m}_{ij,p} = \sigma_0^2\tilde{f}_{ij,p}/(\tilde{\sigma}_{2,ij,p}^2 + \sigma_0^2)$, respectively. For arbitrary chosen initial values of $\tilde{c}_{ij}^{(0)}$, $\tilde{k}_{ij,p}^{(0)}$, $\tilde{f}_{ij,p}^{(0)}$, $\tilde{\theta}_{0,ij}^{(0)}$, $\tilde{C}_{F_{ij}}^{(0)}$, and $\tilde{\vartheta}_{F_{ij}}^{(0)}$, the new estimates of $\tilde{c}_{ij}^{(l+1)}$, $\tilde{k}_{ij,p}^{(l+1)}$, $\tilde{f}_{ij,p}^{(l+1)}$, $\tilde{\theta}_{0,ij}^{(l+1)}$, $\tilde{C}_{F_{ij}}^{(l+1)}$, and $\tilde{\vartheta}_{F_{ij}}^{(l+1)}$ at every iteration l ($l = 0, 1, \ldots$) are obtained according to the optimisation problem in (13), as shown at the bottom of the next page.

In the following, we will provide a detailed step by step explanation of the proposed estimation method.

Step A.1: For fixed values of $\tilde{k}_{ij,p}^{(l)}, \tilde{f}_{ij,p}^{(l)}, \tilde{\theta}_{0,ij}^{(l)}, \tilde{C}_{F_{ij}}^{(l)}$, and $\tilde{\vartheta}_{F_{ij}}^{(l)}$, it can be shown that (13) is minimized if $x = \tilde{c}_{ij}^{(l+1)}$ satisfies the following equation

$$\begin{aligned} 2x^3\left\|\mathbf{y}_{ij}^{(l)}\right\|_2^2 + 3x^2\left(\mathbf{y}_{ij}^{(l)}\right)^T\mathbf{f}_{ij}^{(l)} + x\left[\left|\left|\mathbf{f}_{ij}^{(l)}\right|\right|_2^2 - 2\left(\hat{\mathbf{s}}_{ij} - \mathbf{g}^{(l)}\right)^T\mathbf{y}_{ij}^{(l)}\right] \\ = \left(\mathbf{f}_{ij}^{(l)}\right)^T\left(\hat{\mathbf{s}}_{ij} - \mathbf{g}^{(l)}\right) \end{aligned} \quad (14)$$

where $(\cdot)^T$ represents the transpose operator. In (14), the symbols $\mathbf{g}^{(l)}$, $\mathbf{f}_{ij}^{(l)}$, and $\mathbf{y}_{ij}^{(l)}$ are column vectors containing the stacked values of the functions $(\tilde{C}_{F_{ij}}^{(l)})^2\ G(f_q, 0, \sigma_0^2/2)$, $2\tilde{C}_{F_{ij}}^{(l)}\Re\{G(f_q, \tilde{f}_{ij,p}^{(l)}, (\tilde{\sigma}_{2,ij,p}^{(l)})^2)G^*(f_q, 0, \sigma_0^2)\ \exp(j(\theta_{ij,p}^{(l)} - \tilde{\vartheta}_{F_{ij}}^{(l)}))\}/(\sigma_w\sqrt{\pi})$, and $G(f_q, \tilde{f}_{ij,p}^{(l)}, (\tilde{\sigma}_{1,ij,p}^{(l)})^2)$ for increasing values of q, respectively. Since (14) has real-valued coefficients, at least one of its roots is real. The exact number of real or/and complex roots of (14) are determined by the sign of the corresponding discriminant Δ_0, the expression of which is given in (15), as shown at the bottom of the next page. If $\Delta_0 < 0$ ($\Delta_0 \geq 0$), the cubic equation in (14) has one real root and two complex conjugate roots (three real roots). In all cases, the roots x_k, $k = 1, 2, 3$, are expressed as $x_k = -(b_0 + \zeta^k A_0 + B_0/(\zeta^k A_0))/(3a_0)$, where $\zeta = 0.5(j\sqrt{3} - 1)$ is a cube root of unity, $a_0 = 2||\mathbf{y}_{ij}^{(l)}||_2^2$, $b_0 = 3(\mathbf{y}_{ij}^{(l)})^T\mathbf{f}_{ij}^{(l)}$,

$B_0 = b_0^2 - 3a_0[(||\mathbf{f}_{ij}^{(l)}||^2 - 2(\hat{\mathbf{s}}_{ij,p} - \mathbf{g}^{(l)})^T \mathbf{y}_{ij}^{(l)}]$, and $A_0 = [(C_0 \pm \sqrt{-27\Delta_0\, a_0^2})/2]^{1/3}$, in which $C_0 = 2b_0^2 - 9a_0 b_0[(||\mathbf{f}_{ij}^{(l)}||^2 - 2(\hat{\mathbf{s}}_{ij,p} - \mathbf{g}^{(l)})^T \mathbf{y}_{ij}^{(l)}] - 27a_0^2(\mathbf{f}_{ij}^{(l)})^T(\hat{\mathbf{s}}_{ij,p}^{(l)} - \mathbf{g}^{(l)})$. The new estimate of the path gain $\tilde{c}_{ij}^{(l+1)}$ corresponds to the real-valued root x_k that is a global minimum of the right-hand side of (13). By inserting the new estimate of $\tilde{c}_{ij}^{(l+1)}$ in (13), the optimization problem in (13) reduces to the one in (16), as shown at the bottom of the page.

Step A.2: Then, by deriving the right-hand side of (16) with respect to the variable $\tilde{C}_{F_{ij}}$, it can be shown that the new estimate of $x = \tilde{C}_{F_{ij}}^{(l+1)}$ of the overall path gain of the fixed scatterers satisfies the following equation

$$3x^2\mathbf{j}^T\mathbf{k}_{ij}^{(l)} + x\left[\left|\left|\mathbf{k}_{ij}^{(l)}\right|\right|_2^2 - 2\left(\hat{\mathbf{s}}_{ij,p} - \left(\tilde{c}_{ij}^{(l+1)}\right)^2 \mathbf{y}_{ij}^{(l)}\right)^T \mathbf{j}\right] + 2x^3\,||\mathbf{j}||_2^2 = \left(\mathbf{k}_{ij}^{(l)}\right)^T \left(\hat{\mathbf{s}}_{ij,p} - \left(\tilde{c}_{ij}^{(l+1)}\right)^2 \mathbf{y}_{ij}^{(l)}\right) \quad (17)$$

where $\mathbf{j}$ and $\mathbf{k}_{ij}^{(l)}$ are column vectors containing the stacked values of the functions $G(f_q, 0, \sigma_0^2/2)$ and $2\Re\{G(f, f_{ij,p}^{(l)}, (\sigma_{2,ij,p}^{(l)})^2) G^*(f, 0, \sigma_0^2) \exp(j(\theta_{ij,p}^{(l)} - \vartheta_{F_{ij}}^{(l)}))\}\tilde{c}_{ij}^{(l+1)}/(\sigma_w\sqrt{\pi})$ for increasing values of q, respectively. The number of the real and complex roots of (17) are determined by the sign of its discriminant Δ_1 expressed in (18), as shown at the bottom of the next page. Regardless of the sign of Δ_1, the roots x_k, $k = 1, 2, 3$, of (17) are expressed according to $x_k = -(b_1 + \zeta^k A_1 + B_1/(\zeta^k A_1))/(3a_1)$, where $a_1 = 2||\mathbf{j}||_2^2$, $b_1 = 3\mathbf{j}^T\mathbf{k}_{ij}^{(l)}$, $B_1 = b_1^2 - 3a_1[||\mathbf{k}_{ij}^{(l)}||_2^2 - 2(\hat{\mathbf{s}}_{ij,p} - (\tilde{c}_{ij}^{(l+1)})^2\mathbf{y}_{ij}^{(l)})^T\mathbf{j}]$, and $A_1 = [(C_1 \pm \sqrt{-27\Delta_1\, a_1^2})/2]^{1/3}$, in which $C_1 = 2b_1^3 - 9a_1 b_1[||\mathbf{k}_{ij}^{(l)}||_2^2 - 2(\hat{\mathbf{s}}_{ij,p} - (\tilde{c}_{ij}^{(l+1)})^2\mathbf{y}_{ij}^{(l)})^T\mathbf{j}] - 27a_1^2(\mathbf{k}_{ij}^{(l)})^T(\hat{\mathbf{s}}_{ij,p} - (\tilde{c}_{ij}^{(l+1)})^2\mathbf{y}_{ij}^{(l)})$. The new estimate of the gains $\tilde{C}_{F_{ij}}^{(l+1)}$ is the non-negative real-valued root x_k of (17) that is a global minimum of the right-hand side of (13). By substituting $\tilde{C}_{F_{ij}}^{(l+1)}$ in (13), the optimization problem in (13) reduces to the four-dimensional optimization problem given by (19), as shown at the bottom of the next page.

Step A.3: The new estimates of the TV Doppler frequencies $f_{ij,p}^{(l+1)}$, $i, j = 1, 2$, are obtained by means of the approximate solution to the instantaneous Doppler shift $B_{ij,p}^{(1)} = B_{ij}^{(1)}(t_p)$ in (10) as in (20), as shown at the bottom of the next page. Substituting the approximate solution of the TV Doppler frequencies $f_{ij,p}^{(l+1)}$ in (19) yields the simplified three-dimensional problem given in (21), as shown at the bottom of the next page.

Step A.4: By utilizing (3), an exact expression for the new estimate of the initial phase of the channel $\tilde{\theta}_{0,ij}^{(l+1)}$, $i, j = 1, 2$, can be obtained as

$$\tilde{\theta}_{0,ij}^{(l+1)} = \pm \arccos\left(\frac{\hat{R}_{ij}^2(t_p) - \left(\tilde{c}_{ij}^{(l+1)}\right)^2 - \left(\tilde{C}_{F_{ij}}^{(l+1)}\right)^2}{2\tilde{c}_{ij}^{(l+1)}\tilde{C}_{F_{ij}}^{(l+1)}}\right) + \tilde{\vartheta}_{F_{ij}}^{(l)} - 2\pi\int_0^{t_p} \tilde{f}_{ij,p}^{(l+1)}\,du_p + 2k\pi \quad (22)$$

where the integer k ($k \in \mathbb{Z}$) is introduced to ensure that the optimal solution is within the interval $[0, 2\pi)$. Here, the new estimate of $\tilde{\theta}_{0,ij}^{(l+1)}$ corresponds to the quantity that minimizes

$$\left(\tilde{c}_{ij}^{(l+1)}, \tilde{k}_{ij,p}^{(l+1)}, \tilde{f}_{ij,p}^{(l+1)}, \tilde{\theta}_{0,ij}^{(l+1)}, \tilde{C}_{F_{ij}}^{(l+1)}, \tilde{\vartheta}_{F_{ij}}^{(l+1)}\right) = \underset{\mathcal{P}_1(t_p)}{\operatorname{argmin}} \left|\left|\hat{\mathbf{s}}_{ij,p} - \tilde{c}_{ij}^2 G\left(f_q, \tilde{f}_{ij,p}, \tilde{\sigma}_{1,ij,p}^2\right) - G\left(f_q, 0, \frac{\sigma_0^2}{2}\right)\tilde{C}_{F_{ij}}^2 - \frac{2\tilde{c}_{ij}\tilde{C}_{F_{ij}}}{\sigma_w\sqrt{\pi}}\Re\left\{\frac{\tilde{g}_{ij,p}}{\tilde{\sigma}_{3,ij,p}\sqrt{2\pi}}\exp\left(-\frac{(f_q - \tilde{m}_{ij,p})^2}{2\tilde{\sigma}_{3,ij,p}^2}\right)\exp\left(j\left(\tilde{\theta}_{ij,p} - \tilde{\vartheta}_{F_{ij}}\right)\right)\right\}\right|\right|_2^2. \quad (13)$$

$$\Delta_0 = 108\left|\left|\mathbf{y}_{ij}^{(l)}\right|\right|_2^2\left[2\left(\hat{\mathbf{s}}_{ij,p} - \mathbf{g}^{(l)}\right)^T\mathbf{y}_{ij}^{(l)} - \left|\left|\mathbf{f}_{ij}^{(l)}\right|\right|_2^2\right]\left|\left|\mathbf{f}_{ij}^{(l)}\right|\right|_2^2\left(\mathbf{y}_{ij}^{(l)}\right)^T\left(\hat{\mathbf{s}}_{ij,p} - \mathbf{g}^{(l)}\right) + 108\left(\left(\mathbf{y}_{ij}^{(l)}\right)^T\mathbf{f}_{ij}^{(l)}\right)^3\left(\mathbf{f}_{ij}^{(l)}\right)^T\left(\hat{\mathbf{s}}_{ij,p} - \mathbf{g}^{(l)}\right) + 9\left(\left(\mathbf{y}_{ij}^{(l)}\right)^T\mathbf{f}_{ij}^{(l)}\left[\left|\left|\mathbf{f}_{ij}^{(l)}\right|\right|_2^2 - 2\left(\hat{\mathbf{s}}_{ij,p} - \mathbf{g}^{(l)}\right)^T\mathbf{y}_{ij}^{(l)}\right]\right)^2 - 8\left|\left|\mathbf{y}_{ij}^{(l)}\right|\right|_2^2\left[\left|\left|\mathbf{f}_{ij}^{(l)}\right|\right|_2^2 - 2\left(\hat{\mathbf{s}}_{ij,p} - \mathbf{g}^{(l)}\right)^T\mathbf{y}_{ij}^{(l)}\right]^3 - 108\left|\left|\mathbf{y}_{ij}^{(l)}\right|\right|_2^4\left(\left(\mathbf{f}_{ij}^{(l)}\right)^T\left(\hat{\mathbf{s}}_{ij,p} - \mathbf{g}^{(l)}\right)\right)^2. \quad (15)$$

$$\left(\tilde{k}_{ij,p}^{(l+1)}, \tilde{f}_{ij,p}^{(l+1)}, \tilde{\theta}_{0,ij}^{(l+1)}, \tilde{C}_{F_{ij}}^{(l+1)}, \tilde{\vartheta}_{F_{ij}}^{(l+1)}\right) = \underset{\tilde{k}_{ij,p}, \tilde{f}_{ij,p}, \tilde{\theta}_{0,ij}, \tilde{C}_{F_{ij}}, \tilde{\vartheta}_{F_{ij}}}{\operatorname{argmin}} \left|\left|\hat{\mathbf{s}}_{ij,p} - \left(\tilde{c}_{ij}^{(l+1)}\right)^2 G\left(f_q, \tilde{f}_{ij,p}, \tilde{\sigma}_{1,ij,p}^2\right) - G\left(f_q, 0, \frac{\sigma_0^2}{2}\right)\tilde{C}_{F_{ij}}^2 - \frac{2\tilde{c}_{ij}^{(l+1)}\tilde{C}_{F_{ij}}}{\sigma_w\sqrt{\pi}}\Re\left\{\frac{\tilde{g}_{ij,p}}{\tilde{\sigma}_{3,ij,p}\sqrt{2\pi}}\exp\left(-\frac{(f_q - \tilde{m}_{ij,p})^2}{2\tilde{\sigma}_{3,ij,p}^2}\right)\exp\left(j\left(\tilde{\theta}_{ij,p} - \tilde{\vartheta}_{F_{ij}}\right)\right)\right\}\right|\right|_2^2. \quad (16)$$

the right-hand side of (21). By inserting (22) in (21), the optimization problem reduces to the two-dimensional problem in (23), as shown at the bottom of the next page.

Step A.5: Finally, the new estimates of $\tilde{k}_{ij,p}^{(l+1)}$ and $\tilde{\vartheta}_{F_{ij}}^{(l+1)}$ are determined numerically by minimizing the right-hand side of (23).

It should be stressed that the iterative processes described in Steps A.1−A.5 proceed as long as the relative change in the object function $E_1\left(\mathcal{P}_1(t_p)\right)$ (the absolute value of the difference of the objective function computed at iteration $l+1$ with that at l) is greater than a predefined error level ε_1. Additionally, since indoor channels are non-stationary, these iterative approaches must be carried out at each time instant t_p. In the following subsection, we will estimate the velocity $\vec{v}(t_p)$ of the moving person based on the estimated TV Doppler frequencies $\tilde{f}_{ij,p} = \tilde{f}_{ij}(t_p)$ $(i, j = 1, 2)$.

B. ESTIMATION OF THE TIME-VARIANT VELOCITY

The main purpose of this section is to estimate the TV velocity $\vec{v}(t_p)$, i.e., TV speed $v(t_p)$ and TV AOM $\alpha_v(t_p)$ of the person moving in the considered indoor environment. In the following, the estimated values of $v_p = v(t_p)$, $\alpha_{v,p} = \alpha_v(t_p)$, $\alpha_{j,p}^T = \alpha_j^T(t_p)$, and $\alpha_{i,p}^R = \alpha_i^R(t_p)$ will be denoted by $\tilde{v}_p$, $\tilde{\alpha}_{v,p}$, $\tilde{\alpha}_{j,p}^T$, and $\tilde{\alpha}_{i,p}^R$, respectively.

Here, the problem is to determine a set of parameters $\mathcal{P}_2(t_p) = \left\{\tilde{v}_p, \tilde{\alpha}_{v,p}, \tilde{\alpha}_{i,p}^R, \tilde{\alpha}_{j,p}^T\right\}$ in such a way that the estimated Doppler frequencies $\tilde{f}_{ij,p}$ are as close as possible to those of the simulation model. To do so, we introduce the objective function $E_2\left(\mathcal{P}_2(t_p)\right)$ as

$$E_2\left(\mathcal{P}_2(t_p)\right) = \left\| \begin{matrix} \tilde{f}_{11,p} - f\left(\tilde{v}_p, \tilde{\alpha}_{1,p}^T, \tilde{\alpha}_{1,p}^R, \tilde{\alpha}_v\right) \\ \tilde{f}_{12,p} - f\left(\tilde{v}_p, \tilde{\alpha}_{2,p}^T, \tilde{\alpha}_{1,p}^R, \tilde{\alpha}_v\right) \\ \tilde{f}_{21,p} - f\left(\tilde{v}_p, \tilde{\alpha}_{2,p}^T, \tilde{\alpha}_{1,p}^R, \tilde{\alpha}_v\right) \\ \tilde{f}_{11,p} - f\left(\tilde{v}_p, \tilde{\alpha}_{2,p}^T, \tilde{\alpha}_{2,p}^R, \tilde{\alpha}_v\right) \end{matrix} \right\|_2^2 \tag{24}$$

where $f(a, b, c, d) = -f_0\ a\left[\cos(b-d)+\cos(c-d)\right]/c_0$. With respect to the Euclidean norm described in (24), the optimal values of the set of parameters $\mathcal{P}_2(t_p)$ will be determined

$$\begin{aligned} \Delta_1 = & -108\left|\left|\mathbf{j}\right|\right|_2^2 \mathbf{j}^T \mathbf{k}_{ij}^{(l)} \left[\left|\left|\mathbf{k}_{ij}^{(l)}\right|\right|_2^2 - 2\left(\hat{\mathbf{s}}_{ij,p} - \left(\tilde{c}_{ij}^{(l+1)}\right)^2 \mathbf{y}_{ij}^{(l)}\right)^T \mathbf{j}\right] \left(\mathbf{k}_{ij}^{(l)}\right)^T \left(\hat{\mathbf{s}}_{ij,p} - \left(\tilde{c}_{ij}^{(l+1)}\right)^2 \mathbf{y}_{ij}^{(l)}\right) \\ & + 108\left(\mathbf{j}^T \mathbf{k}_{ij}^{(l)}\right)^3 \left(\mathbf{k}_{ij}^{(l)}\right)^T \left(\hat{\mathbf{s}}_{ij,p} - \left(\tilde{c}_{ij}^{(l+1)}\right)^2 \mathbf{y}_{ij}^{(l)}\right) + 9\left(\mathbf{j}^T \mathbf{k}_{ij}^{(l)} \left[\left|\left|\mathbf{k}_{ij}^{(l)}\right|\right|_2^2 - 2\left(\hat{\mathbf{s}}_{ij,p} - \left(\tilde{c}_{ij}^{(l+1)}\right)^2 \mathbf{y}_{ij}^{(l)}\right)^T \mathbf{j}\right]\right)^2 \\ & - 8\left|\left|\mathbf{j}\right|\right|_2^2 \left[\left|\left|\mathbf{k}_{ij}^{(l)}\right|\right|_2^2 - 2\left(\hat{\mathbf{s}}_{ij,p} - \left(\tilde{c}_{ij}^{(l+1)}\right)^2 \mathbf{y}_{ij}^{(l)}\right)^T \mathbf{j}\right]^3 - 108\left|\left|\mathbf{j}\right|\right|_2^4 \left(\left(\mathbf{k}_{ij}^{(l)}\right)^T \left(\hat{\mathbf{s}}_{ij,p} - \left(\tilde{c}_{ij}^{(l+1)}\right)^2 \mathbf{y}_{ij}^{(l)}\right)\right)^2. \end{aligned} \tag{18}$$

$$\begin{aligned} \left(\tilde{k}_{ij,p}^{(l+1)}, \tilde{f}_{ij,p}^{(l+1)}, \tilde{\theta}_{0,ij}^{(l+1)}, \tilde{\vartheta}_{F_{ij}}^{(l+1)}\right) = \underset{\tilde{k}_{ij,p}, \tilde{f}_{ij,p}, \tilde{\theta}_{0,ij}, \tilde{\vartheta}_{F_{ij}}}{\operatorname{argmin}} & \left|\left|\hat{\mathbf{s}}_{ij,p} - \left(\tilde{c}_{ij}^{(l+1)}\right)^2 G\left(f_q, \tilde{f}_{ij,p}, \tilde{\sigma}_{1,ij,p}^2\right) - G\left(f_q, 0, \frac{\sigma_0^2}{2}\right)\left(\tilde{C}_{F_{ij}}^{(l+1)}\right)^2 \right.\right. \\ & \left.\left. - \frac{2\tilde{c}_{ij}^{(l+1)} \tilde{C}_{F_{ij}}^{(l+1)}}{\sigma_w \sqrt{\pi}} \Re\left\{\frac{\tilde{g}_{ij,p}}{\tilde{\sigma}_{3,ij,p}\sqrt{2\pi}} \exp\left(-\frac{\left(f_q - \tilde{m}_{ij,p}\right)^2}{2\tilde{\sigma}_{3,ij,p}^2}\right) \exp\left(j\left(\tilde{\theta}_{ij,p} - \tilde{\vartheta}_{F_{ij}}\right)\right)\right\}\right|\right|_2^2. \end{aligned} \tag{19}$$

$$f_{ij,p}^{(l+1)} \approx \frac{B_{ij,p}^{(1)}\left[\left(\tilde{c}_{ij}^{(l+1)}\right)^2 + \left(\tilde{C}_{F_{ij}}^{(l+1)}\right)^2 + \frac{\sqrt{2}\tilde{c}_{ij}^{(l+1)} \tilde{C}_{F_{ij}}^{(l+1)}}{\sigma_w \pi} \Re\left\{\left(\left(\tilde{\sigma}_{2,ij}^{(l)}\right)^2 + \sigma_0^2\right)^{-\frac{1}{2}} \exp\left(j\left(\tilde{\theta}_{ij,p} - \tilde{\vartheta}_{F_{ij}}\right)\right)\right\}\right]}{\left(\tilde{c}_{ij}^{(l+1)}\right)^2 - \frac{\sqrt{2}\tilde{c}_{ij}^{(l+1)} \tilde{C}_{F_{ij}}^{(l+1)} \sigma_0^2}{\sigma_w \pi} \Re\left\{\left(\left(\tilde{\sigma}_{2,ij}^{(l)}\right)^2 + \sigma_0^2\right)^{-\frac{3}{2}} \exp\left(j\left(\tilde{\theta}_{ij,p}^{(l)} - \tilde{\vartheta}_{F_{ij}}^{(l)}\right)\right)\right\}}. \tag{20}$$

$$\begin{aligned} \left(\tilde{k}_{ij,p}^{(l+1)}, \tilde{\theta}_{0,ij}^{(l+1)}, \tilde{\vartheta}_{F_{ij}}^{(l+1)}\right) = \underset{\tilde{k}_{ij,p}, \tilde{\theta}_{0,ij}, \tilde{\vartheta}_{F_{ij}}}{\operatorname{argmin}} & \left|\left|\hat{\mathbf{s}}_{ij,p} - \left(\tilde{c}_{ij}^{(l+1)}\right)^2 G\left(f_q, \tilde{f}_{ij,p}, \tilde{\sigma}_{1,ij,p}^2\right) - G\left(f_q, 0, \frac{\sigma_0^2}{2}\right)\left(\tilde{C}_{F_{ij}}^{(l+1)}\right)^2 \right.\right. \\ & \left.\left. - \frac{2\tilde{c}_{ij}^{(l+1)} \tilde{C}_{F_{ij}}^{(l+1)}}{\sigma_w \sqrt{\pi}} \Re\left\{\frac{\tilde{g}_{ij,p}}{\tilde{\sigma}_{3,ij,p}\sqrt{2\pi}} \exp\left(-\frac{\left(f_q - \tilde{m}_{ij,p}\right)^2}{2\tilde{\sigma}_{3,ij,p}^2}\right) \exp\left(j\left(\tilde{\theta}_{ij,p} - \tilde{\vartheta}_{F_{ij}}\right)\right)\right\}\right|\right|_2^2. \end{aligned} \tag{21}$$

by fitting the estimated Doppler frequencies $\tilde{f}_{ij,p}$ as close as possible to the output of the function $f\left(\tilde{v}_p, \tilde{\alpha}_{j,p}^T, \tilde{\alpha}_{i,p}^R, \tilde{\alpha}_{v,p}\right)$.

Step B.1: The initial values of $\tilde{v}_p^{(0)}$, $\tilde{\alpha}_{v,p}^{(0)}$, $(\tilde{\alpha}_{i,p}^R)^{(0)}$ and $(\tilde{\alpha}_{j,p}^T)^{(0)}$ are chosen arbitrary. Then, the new estimates of the speed $\tilde{v}_p^{(l+1)}$, AOM $\tilde{\alpha}_{v,p}^{(l+1)}$, AOD $(\tilde{\alpha}_{j,p}^T)^{(l+1)}$ $(j = 1, 2)$, and AOA $(\tilde{\alpha}_{i,p}^R)^{(l+1)}$ $(i = 1, 2)$ are obtained according to

$$\left(\tilde{v}_p^{(l+1)}, \tilde{\alpha}_{v,p}^{(l+1)}, \left(\tilde{\alpha}_{1,p}^T\right)^{(l+1)}, \left(\tilde{\alpha}_{2,p}^T\right)^{(l+1)}, \left(\tilde{\alpha}_{1,p}^R\right)^{(l+1)}, \left(\tilde{\alpha}_{2,p}^R\right)^{(l+1)}\right) = \underset{\mathcal{P}_2(t_p)}{\operatorname{argmin}} \left\| \begin{vmatrix} \tilde{f}_{11,p} - f\left(\tilde{v}_p, \tilde{\alpha}_{1,p}^T, \tilde{\alpha}_{1,p}^R, \tilde{\alpha}_{v,p}\right) \\ \tilde{f}_{12,p} - f\left(\tilde{v}_p, \tilde{\alpha}_{2,p}^T, \tilde{\alpha}_{1,p}^R, \tilde{\alpha}_{v,p}\right) \\ \tilde{f}_{21,p} - f\left(\tilde{v}_p, \tilde{\alpha}_{1,p}^T, \tilde{\alpha}_{2,p}^R, \tilde{\alpha}_{v,p}\right) \\ \tilde{f}_{22,p} - f\left(\tilde{v}_p, \tilde{\alpha}_{2,p}^T, \tilde{\alpha}_{2,p}^R, \tilde{\alpha}_{v,p}\right) \end{vmatrix} \right\|_2^2 . \tag{25}$$

By deriving the right-hand side of (25), it can be shown that (25) is minimized if the new estimate of the speed $\tilde{v}_p^{(l+1)}$ is expressed as (26), as shown at the bottom of the next page.

By substituting (26) in (25), the estimation problem in (25) reduces to

$$\left(\tilde{\alpha}_{v,p}^{(l+1)}, \left(\tilde{\alpha}_{1,p}^T\right)^{(l+1)}, \left(\tilde{\alpha}_{2,p}^T\right)^{(l+1)}, \left(\tilde{\alpha}_{1,p}^R\right)^{(l+1)}, \left(\tilde{\alpha}_{2,p}^R\right)^{(l+1)}\right) = \underset{P_2(t_p)\setminus\{\tilde{v}_p\}}{\operatorname{argmin}} \left\| \begin{vmatrix} \tilde{f}_{11,p} - f\left(\tilde{v}_p^{(l+1)}, \tilde{\alpha}_{1,p}^T, \tilde{\alpha}_{1,p}^R, \tilde{\alpha}_{v,p}\right) \\ \tilde{f}_{12,p} - f\left(\tilde{v}_p^{(l+1)}, \tilde{\alpha}_{2,p}^T, \tilde{\alpha}_{1,p}^R, \tilde{\alpha}_{v,p}\right) \\ \tilde{f}_{21,p} - f\left(\tilde{v}_p^{(l+1)}, \tilde{\alpha}_{1,p}^T, \tilde{\alpha}_{2,p}^R, \tilde{\alpha}_{v,p}\right) \\ \tilde{f}_{22,p} - f\left(\tilde{v}_p^{(l+1)}, \tilde{\alpha}_{2,p}^T, \tilde{\alpha}_{2,p}^R, \tilde{\alpha}_{v,p}\right) \end{vmatrix} \right\|_2^2 . \tag{27}$$

Step B.2: Then, it can be shown that the estimates of the AODs $x = \left(\tilde{\alpha}_{j,p}^T\right)^{(l+1)}$ satisfy

$$\left[\frac{f_0 \tilde{v}_p^{(l+1)}}{c_0}\left[2\cos\left(x - \tilde{\alpha}_v\right) + \cos\left(\tilde{\alpha}_{1,p}^R - \tilde{\alpha}_{v,p}\right) + \cos\left(\tilde{\alpha}_{2,p}^R - \tilde{\alpha}_{v,p}\right)\right] + \tilde{f}_{1j,p} + \tilde{f}_{2j,p}\right] \sin\left(x - \tilde{\alpha}_{v,p}\right) = 0. \tag{28}$$

The equation in (28) has three roots x_0 and $x_{1,\pm}$ which are expressed as

$$x_0 = \tilde{\alpha}_v + k\pi \tag{29}$$

and

$$x_{1,\pm} = \pm \arccos\left[-\frac{1}{2}\left[c_0 \frac{\tilde{f}_{1j,p} + \tilde{f}_{2j,p}}{f_0 \tilde{v}_p^{(l+1)}} + \cos\left(\tilde{\alpha}_{1,p}^R - \tilde{\alpha}_{v,p}\right) + \cos\left(\tilde{\alpha}_{2,p}^R - \tilde{\alpha}_{v,p}\right)\right] + \tilde{\alpha}_{v,p}\right] + 2k\pi \tag{30}$$

for $k \in \mathbb{Z}$, respectively. The new estimate of $\left(\tilde{\alpha}_{j,p}^T\right)^{(l+1)}$ corresponds to the root that is a global minimum of the right-hand side of (27). Similarly, the estimates of the AOAs $x = \left(\tilde{\alpha}_{i,p}^R\right)^{(l+1)}$ satisfy

$$\left[\frac{f_0 \tilde{v}_p^{(l+1)}}{c_0}\left[2\cos\left(x - \tilde{\alpha}_{v,p}\right) + \cos\left(\tilde{\alpha}_{1,p}^T - \tilde{\alpha}_{v,p}\right) + \cos\left(\tilde{\alpha}_{2,p}^T - \tilde{\alpha}_{v,p}\right)\right] + \tilde{f}_{i1,p} + \tilde{f}_{i2,p}\right] \sin\left(x - \tilde{\alpha}_{v,p}\right) = 0. \tag{31}$$

The equation in (31) has three roots x_0 and $x_{2,\pm}$, where

$$x_{2,\pm} = \pm \arccos\left[-\frac{1}{2}\left[c_0 \frac{\tilde{f}_{i1,p} + \tilde{f}_{i2,p}}{f_0 \tilde{v}_p^{(l+1)}} + \cos\left(\tilde{\alpha}_{1,p}^T - \tilde{\alpha}_{v,p}\right) + \cos\left(\tilde{\alpha}_{2,p}^T - \tilde{\alpha}_{v,p}\right)\right] + \tilde{\alpha}_{v,p}\right] + 2k\pi \tag{32}$$

for $k \in \mathbb{Z}$, respectively. The new estimate of $\left(\tilde{\alpha}_{i,p}^R\right)^{(l+1)}$ correspond to the root that is a global minimum of the right-hand side of (27). It should be stressed that the integer k in (29), (30), and (32) is introduced to ensure that the solutions x_0, $x_{1,\pm}$, and $x_{2,\pm}$ are within the interval $[0, 2\pi)$.

Step B.3: Finally, replacing the new estimates of the AOAs and AOD in (27) leads to the following one-dimensional optimization procedure

$$\tilde{\alpha}_{v,p}^{(l+1)} = \underset{\tilde{\alpha}_{v,p}}{\operatorname{argmin}} \left\| \begin{vmatrix} \tilde{f}_{11,p} - f\left(\tilde{v}_p^{(l+1)}, \left(\tilde{\alpha}_{1,p}^T\right)^{(l+1)}, \left(\tilde{\alpha}_{1,p}^R\right)^{(l+1)}, \tilde{\alpha}_{v,p}\right) \\ \tilde{f}_{12,p} - f\left(\tilde{v}_p^{(l+1)}, \left(\tilde{\alpha}_{2,p}^T\right)^{(l+1)}, \left(\tilde{\alpha}_{1,p}^R\right)^{(l+1)}, \tilde{\alpha}_{v,p}\right) \\ \tilde{f}_{21,p} - f\left(\tilde{v}_p^{(l+1)}, \left(\tilde{\alpha}_{1,p}^T\right)^{(l+1)}, \left(\tilde{\alpha}_{2,p}^R\right)^{(l+1)}, \tilde{\alpha}_{v,p}\right) \\ \tilde{f}_{22,p} - f\left(\tilde{v}_p^{(l+1)}, \left(\tilde{\alpha}_{2,p}^T\right)^{(l+1)}, \left(\tilde{\alpha}_{2,p}^R\right)^{(l+1)}, \tilde{\alpha}_{v,p}\right) \end{vmatrix} \right\|_2^2 . \tag{33}$$

The iterative procedure described in Steps B.1−B.3, proceeds as long as the object function $E_2\left(\mathcal{P}_2(t_p)\right)$ is higher than

$$\left(\tilde{k}_{ij,p}^{(l+1)}, \tilde{\vartheta}_{F_{ij}}^{(l+1)}\right) = \underset{\tilde{k}_{ij,p}, \tilde{\vartheta}_{F_{ij}}}{\operatorname{argmin}} \left\| \hat{\mathbf{s}}_{ij,p} - \left(\tilde{c}_{ij}^{(l+1)}\right)^2 G\left(f_q, \tilde{f}_{ij,p}^{(l+1)}, \tilde{\sigma}_{1,ij,p}^2\right) - \left(\tilde{C}_{F_{ij}}^{(l+1)}\right)^2 G\left(f_q, 0, \frac{\sigma_0^2}{2}\right) - \frac{2\tilde{c}_{ij}^{(l+1)} \tilde{C}_{F_{ij}}^{(l+1)}}{\sigma_w \sqrt{\pi}} \Re\left\{\frac{\tilde{g}_{ij,p}^{(l+1)}}{\tilde{\sigma}_{3,ij,p}\sqrt{2\pi}} \exp\left(-\frac{\left(f_q - \tilde{m}_{ij,p}^{(l+1)}\right)^2}{2\tilde{\sigma}_{3,ij,p}^2}\right) \exp\left(j\left(\tilde{\theta}_{ij,p}^{(l+1)} - \tilde{\vartheta}_{F_{ij}}\right)\right)\right\} \right\|_2^2 . \tag{23}$$

the error threshold ε_2 and must be performed at each time instant t_p.

IV. NUMERICAL RESULTS AND DISCUSSION

A. NUMERICAL RESULTS

In this section, we present the numerical results for the validation of the proposed estimation algorithms by comparing the exact TV Doppler frequencies and TV velocity with the corresponding estimated values. This task calls for prior knowledge of the channel parameters. This information is not available for RF measurement data. The output of sensor-based devices cannot be employed to this end. In fact, although numerous commercial wearable and context-aware devices are available, they do not reflect the exact values of the TV velocity. While estimating the TV displacements and/or TV velocity, such devices introduce their own estimation error. In this case, considering these systems for comparison would do not allow a correct quantitative evaluation of the performance of our algorithm. Therefore, we consider in the following test signals, for which the exact channel parameters are known and which are generated by computer simulations.

For the analysis of the performance of the estimation method, we considered three different scenarios, which we observed over the time interval [0, 5s]. The room is characterized by its length A and width B, which are 14 m and 7 m, respectively. The fixed locations of the transmit and receive antennas A_1^T, A_2^T, A_1^R, and A_2^R are $(-4.9, 1)$, $(-4.9, -1)$, $(4.5, 2)$, and $(4.5, -2)$, respectively. The person in the room stands at the initial position $(1, 2)$, walks then along a linear trajectory. In Scenario I, the person is moving at a constant speed $v_1(t) = 1.1$ m/s. In Scenario II, the motion of the person is comprised of three parts. The person starts by walking with constant speed, decelerates at the time instant $t = 2.5$s, and finally stops at $t = 4.5$s. In this case, the person's speed $v_2(t)$ is

$$v_2(t) = \begin{cases} 1 & if\, 0 \le t \le 2.5s \\ -0.25t+1.125 & if\, 2.5 \le t \le 4.5s \\ 0 & if\, 4.5 \le t \le 5s. \end{cases} \quad (34)$$

Finally, in Scenario III, the speed is modelled using a sinusoidal function and is given by $v_3(t) = 0.3\sin(\pi t/3+0.5)+0.35$. In all scenarios, the AOM has been set to $\pi/3$. The TV speed values of the different scenarios have been chosen in accordance with the study reported in [51]. Here, we consider $M = 7$ fixed scatterers with $\sum_{m=1}^{M} c_m^2 = M\sigma^2 = 1$. Also, the carrier frequency f_0 has been set to 5.9 GHz. The parameter σ_w^2 has been chosen to be $\sigma_w^2 = 1/(6\pi)$. In the following, the error threshold levels ε_1 and ε_2 have been set to 0.0001.

TABLE 1. Average error of the estimated Doppler frequency $\varepsilon_{\text{Doppler}}$ in Hz for various values of the SNR η.

SNR η (dB)	Scenario I	Scenario II	Scenario III
$\eta \longrightarrow \infty$	0.25	0.23	0.24
20	0.31	0.28	0.27
15	0.35	0.32	0.31
10	0.68	0.38	0.33
5	1.16	1.25	1.4
0	4.81	3.81	3.21

TABLE 2. Average error of the estimated speed $\varepsilon_{\text{Speed}}$ in m/s for various values of the SNR η.

SNR η (dB)	Scenario I	Scenario II	Scenario III
$\eta \longrightarrow \infty$	0.02	0.02	0.02
20	0.03	0.02	0.02
15	0.03	0.03	0.03
10	0.06	0.04	0.04
5	0.11	0.15	0.13
0	0.30	0.35	0.32

To ensure realistic applicability, the performance and robustness of our proposed estimation methods should be evaluated in the presence of noise. To this end, we denote by η the average SNR at the receiver side.

The proposed iterative estimation method has been applied to generate the results depicted in Figs. 4 and 5. In Figs. 4 (a)−(c), we compare between the exact TV Doppler frequency $f_{11}(t)$ and the corresponding estimated quantity which has been obtained by applying Steps (1)−(5) described by (13)−(23), for Scenarios I−III with different values of the SNR η. To clarify the figures, the TV Doppler frequencies $f_{12}(t)$, $f_{21}(t)$, and $f_{22}(t)$ have been omitted. However, it should be stressed that analogous results can be observed for the TV Doppler frequencies $f_{12}(t), f_{21}(t)$, and $f_{22}(t)$. The corresponding exact and estimated TV speed $v(t)$ is illustrated in Figs. 5 (a), (b), and (c) for Scenarios I, II, and III, respectively. The good fit between the exact quantities and their estimates observed in Figs. 4 and. 5 confirms the validity of the proposed RF-based estimation technique. Although the accuracy of this estimation method degrades with decreasing values of the SNR η, it is clear from Figs. 4 and. 5, that it is robust against noise for a single generated noise sample. To better examine the noise robustness of the estimation procedure in Section III, we present in Tables 1 and 2 the average Doppler frequency estimation error $\varepsilon_{\text{Doppler}}$ and the average speed estimation error $\varepsilon_{\text{Speed}}$, respectively.

$$\tilde{v}_p^{(l+1)} = \frac{c_0 \sum_{i,j=1}^{2} \tilde{f}_{ij,p} \left[\cos\left(\left(\tilde{\alpha}_{j,p}^{T}\right)^{(l)} - \tilde{\alpha}_{v,p}^{(l)}\right) + \cos\left(\left(\tilde{\alpha}_{i,p}^{R}\right)^{(l)} - \tilde{\alpha}_{v,p}^{(l)}\right)\right]}{f_0 \sum_{i,j=1}^{2} \left[\cos\left(\left(\tilde{\alpha}_{j,p}^{T}\right)^{(l)} - \tilde{\alpha}_{v,p}^{(l)}\right) + \cos\left(\left(\tilde{\alpha}_{i,p}^{R}\right)^{(l)} - \tilde{\alpha}_{v,p}^{(l)}\right)\right]^2}. \quad (26)$$

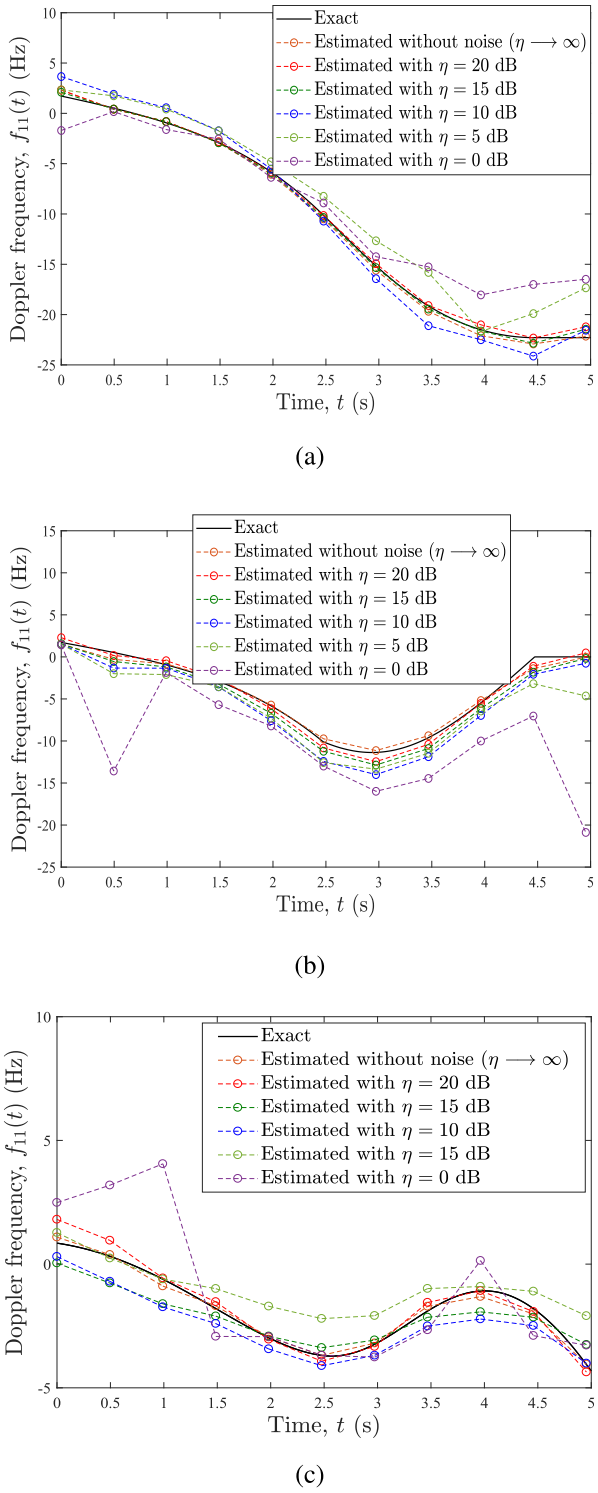

FIGURE 4. Time-variant Doppler frequencies $f_{11}(t)$ for (a) Scenario I (constant speed model), (b) Scenario II (linear speed model), and (c) Scenario III (sinusoidal speed model) with the corresponding estimated values for different values of the SNR η.

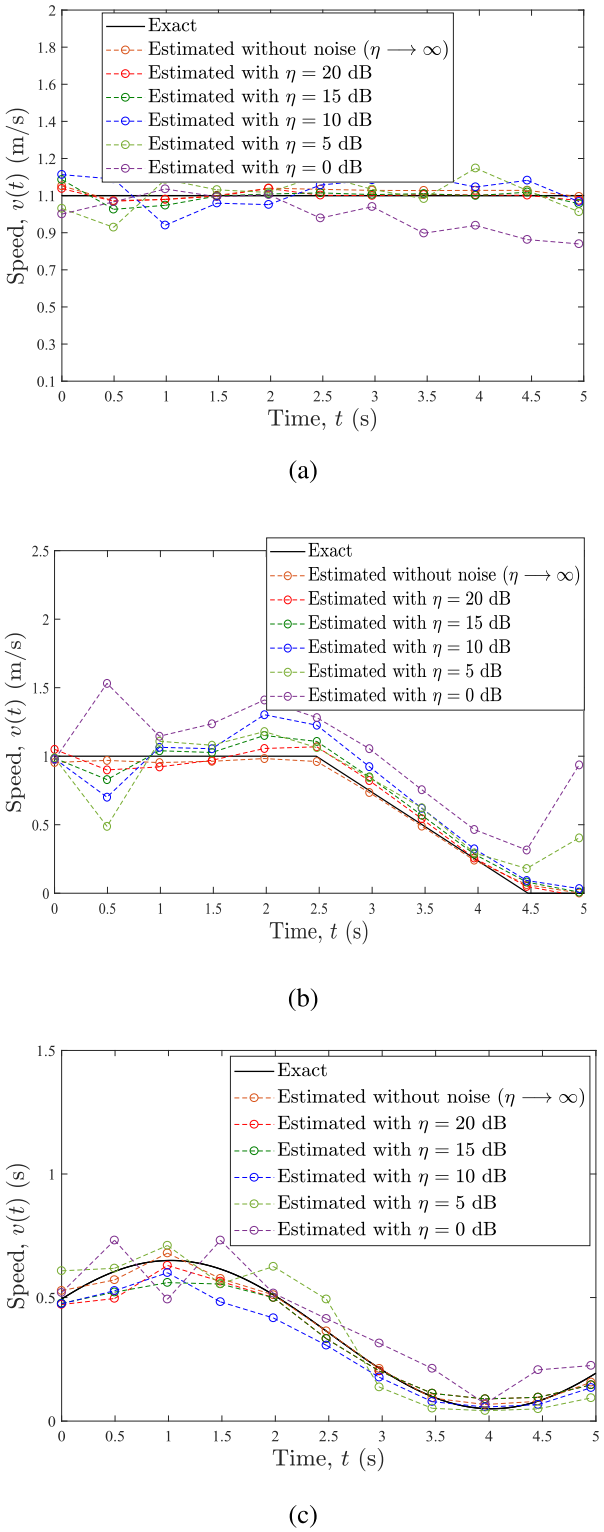

FIGURE 5. Time-variant speed $v(t)$ of the moving scatterer S^M for Scenario I (constant speed model), (b) Scenario II (linear speed model), and (c) Scenario III (sinusoidal speed model) with the corresponding estimated values for different values of the SNR η.

Tables 1 and 2 show that the estimation method allows an accurate estimation of the TV Doppler frequencies $f_{ij}(t)$ $(i, j = 1, 2)$ and TV speed $v(t)$ with an estimation error of approximately 3 % or less, for high values of the SNR, i.e., $\eta \geq 20$ dB for the different scenarios. Furthermore, for $\eta = 15$ dB, the estimation occurs with an accuracy of approximately 97 %. The robustness becomes more evident

for smaller SNR values. In fact, for $\eta = 0$ and assuming an average walking speed of 1 m/s, the speed estimation error is around 30 %.

The robustness of the proposed method against noise can be explained by two factors. First, in this method, the estimates of the instantaneous Doppler frequencies $f_{ij}(t)$ are obtained by means of the TV mean Doppler shift which is determined at each time instant t_p by averaging the spectrogram $S_{ij}(f_q, t_p)$ over the frequencies f_q, thereby reducing the effect of noise. The second factor is that the spectrogram $S_{ij}(f_q, t_p)$ itself is not very sensitive to noise. In fact, as is detailed in [48, Section IV], the spectrogram $S_{ij}(f_q, t_p)$ is obtained by deriving the short-time Fourier transform by integrating the short-time complex channel gain with respect to the running time t' which reduces the effect of noise.

B. COMPARISON WITH EXISTING WORKS

In this section, we will discuss existing works and give reasons why these methods cannot be considered for fair comparison purposes. As it has been mentioned in Section I.A, existing estimation techniques can be divided into two groups: methods developed in the context of mobile radio communications and approaches reported for ADL monitoring.

The estimation techniques proposed in the context of WSS mobile radio channels utilize the statistical properties (e.g., LCR, the covariance, ...) of the fading channel to extract the MSs' speed, which is assumed to be constant during the total observation time. A review of [4] and [18] shows that these methods require priori knowledge of analytical solutions to the higher-order statistics of the underlying multipath fading channel. To the best of the authors' knowledge, the theoretical analysis available in the literature is limited to WSS channels (constant speed), and there exist, to date, no results regarding the statistical characteristics of channels which exhibit a non-stationary behavior.

One method which was developed in the context of velocity-based ADLs monitoring and can be examined for comparison purposes is that described in [29]. However, the details of the employed algorithm are not available and similar results cannot be reproduced.

Other interesting methods can be found in [37]–[40] and are based on wll-known speed estimation procedures developed for WSS channels, such as [39] and IndoTrack [40]. Although of interest, these techniques can only be applied during sub-time intervals where the person is assumed not to move (stationary scenarios, i.e., the channel is assumed to be WSS and the speed is constant). Then, what is computed is the average speed and not the TV speed. Also, they estimate the TV Doppler frequencies and TV delays independently without conforming to the fundamental relationship between them [52] and taking it into account.

Therefore, no comparison results with other mobile radio speed-based algorithms can be presented. The good agreement between the exact and estimated channel parameters (TV speed and TV Doppler frequencies) observed in Figs. 4 and 5 for various speed profiles confirms the validity and robustness of the proposed estimation procedures.

V. CONCLUSION

In the context of velocity-based indoor ADLs monitoring, we introduce in this article a new iterative method to accurately estimate the instantaneous velocity (TV speed and TV AOM) of a single moving person. This person is modelled by a single point moving scatterer and is moving in an indoor area which is equipped with a distributed 2×2 MIMO communication system. The estimation algorithm is comprised of two major parts. In the first part, the estimates of the TV Doppler frequencies are numerically computed by fitting the exact spectrograms of the complex channel gains to those of received radio signals. Subsequently, the desired TV velocity is obtained by exploiting the estimated values of the instantaneous Doppler frequencies. Together with the TV velocity, the proposed method computes all channel parameters, which allows for a better emulation of non-stationary indoor channels. Closed-form solutions have been derived for the path gains and the TV Doppler frequencies as well as the TV speed, and the TV angles, which in turn, greatly simplifies the underlying optimization problems. Numerical results are presented which illustrate the good agreement between the exact TV speed and the resulting TV Doppler frequencies of the moving person and the corresponding estimated quantities. This confirms the validity and accuracy of the proposed estimation procedures for several speed profiles. In addition, the effects of noise have also been studied in detail and it has been shown that these methods are robust against noise. It has been shown that the proposed algorithm estimates the parameters of interest with an accuracy varying from 70% to 97% for SNR values between 0 dB and 20 dB.

APPENDIX

In this appendix, we present the mathematical details leading to the expression of the cross-term $S_{ij}^{(c)}(f, t)$ as described in (6). To do so, we start by showing that the product of the Gaussian functions $G(f, f_{ij}(t), \sigma_{2,ij}^2)$ and $G^*(f, 0, \sigma_0^2)$ is a weighted Gaussian function, the parameters of which will also be determined. Let us denote by $P_g(f, t)$ the product of $G(f, f_{ij}(t), \sigma_{2,ij}^2)$ and $G^*(f, 0, \sigma_0^2)$, i.e., $P_g(f, t) = G(f, f_{ij}(t), \sigma_{2,ij}^2)G^*(f, 0, \sigma_0^2)$. The product $P_g(f, t)$ is expressed as

$$P_g(f, t) = \frac{1}{2\pi\sigma_{2,ij}\sigma_0} \exp\left[-\frac{1}{2}\left(\frac{\left(f - f_{ij}(t)\right)^2}{\sigma_{2,ij}^2} + \frac{f^2}{\sigma_0^2}\right)\right]. \quad (35)$$

By introducing $z = (((f - f_{ij}(t))^2/\sigma_{2,ij}^2) + (f^2/\sigma_0^2))/2$, and performing some mathematical manipulations, the quantity z can be written as

$$z = \frac{\left(f - m_{ij}(t)\right)^2}{2\sigma_{3,ij}^2} + \frac{f_{ij}^2(t)}{2\left(\sigma_{2,ij}^2 + \sigma_0^2\right)} \quad (36)$$

where $m_{ij}(t) = \sigma_0^2 \, f_{ij}(t)/(\sigma_{2,ij}^2+\sigma_0^2)$ and $\sigma_{3,ij}^2 = \sigma_{2,ij}^2\sigma_0^2/(\sigma_{2,ij}^2+\sigma_0^2)$. Then, by inserting (36) in (35), we have that the product $P_g(f,t)$ is a scaled Gaussian PDF expressed as

$$P_g(f,t) = \frac{g_{ij}(t)}{\sigma_{3,ij}\sqrt{2\pi}} \exp\left(-\frac{\left(f-m_{ij}(t)\right)^2}{2\sigma_{3,ij}^2}\right) \tag{37}$$

where the scaling factor $g_{ij}(t)$ is itself a Gaussian PDF on $f_{ij}(t)$ with variance $\sigma_{2,ij}^2+\sigma_0^2$, i.e.,

$$g_{ij}(t) = \frac{1}{\sqrt{2\pi\left(\sigma_{2,ij}^2+\sigma_0^2\right)}} \exp\left(-\frac{f_{ij}^2(t)}{2\left(\sigma_{2,ij}^2+\sigma_0^2\right)}\right). \tag{38}$$

Moreover, by substituting $\sigma_{2,ij}^2 = \sigma_0^2 - jk_{ij}/(2\pi)$ and $\sigma_0^2 = 1/(2\pi\sigma_w)^2$ in (38), and profiting from the facts that $\sigma_w \ll 1$ and σ_w is inversely proportional to k_{ij}, it can easily be shown that both the real and imaginary parts of the expression within the exponential function tend to 0. This result leads to the following approximation of the term $g_{ij}(t)$

$$g_{ij}(t) \approx 1/\sqrt{2\pi\left(\sigma_{2,ij}^2+\sigma_0^2\right)}. \tag{39}$$

ACKNOWLEDGMENT

This article was presented in part at the IEEE Global Communications Conference (GLOBECom'18), Abu Dhabi, United Arab Emirates, December 2018 [1].

REFERENCES

[1] R. Hicheri, M. Patzold, and N. Youssef, "Estimation of the velocity of a walking person in indoor environments from mmWave signals," in *Proc. IEEE Globecom Workshops (GC Wkshps)*, Abu Dhabi, United Arab Emirates, Dec. 2018, pp. 1–7.

[2] Z. Hussain, M. Sheng, and W. Emma Zhang, "Different approaches for human activity recognition: A survey," 2019, *arXiv:1906.05074*. [Online]. Available: http://arxiv.org/abs/1906.05074

[3] G. L. Stüber, *Principles of Mobile Radio Communications*, 2nd ed. Norwell, MA, USA: Kluwer, 2000.

[4] G. Azemi, E. Holmbakken, V. Karawalevu, and B. Senadji, "The importance of accurate velocity estimation in designing handover algorithms for microcellular systems," in *Proc. 4th Australas. Workshop Signal Process. Appl.*, V. Chandran, Ed. Dec. 2002, pp. 163–166.

[5] H. Zhang and A. Abdi, "Mobile speed estimation using diversity combining in fading channels," in *Proc. IEEE Global Commun. Conf. (GLOBECOM)*, Nov./Dec. 2004, pp. 3685–3689.

[6] Y. Zhuang, J. Hua, H. Wen, Y. Meng, and L. Meng, "An iterative Doppler shift estimation in vehicular communication systems," *Procedia Eng.*, vol. 29, pp. 4129–4134, 2012.

[7] A. Sampath and J. M. Holtzman, "Estimation of maximum Doppler frequency for handoff decisions," in *Proc. IEEE 43rd Veh. Technol. Conf. (VTC)*, May 1993, pp. 859–862.

[8] M. D. Austin, "Handoff algorithms and co-channel interference analysis for microcellular systems," Georgia Inst. Technol., Atlanta, GA, USA, Tech. Rep., 1994.

[9] K. D. Anim-Appiah, "On generalized covariance-based velocity estimation," *IEEE Trans. Veh. Technol.*, vol. 48, no. 5, pp. 1546–1557, Sep. 1999.

[10] J. M. Holtzman and A. Sampath, "Adaptive averaging methodology for handoffs in cellular systems," *IEEE Trans. Veh. Technol.*, vol. 44, no. 1, pp. 59–66, Feb. 1995.

[11] C. Tepedelenlioğlu and G. B. Giannakis, "On velocity estimation and correlation properties of narrow-band mobile communication channels," *IEEE Trans. Veh. Technol.*, vol. 50, no. 4, pp. 1039–1052, Jul. 2001.

[12] K. E. Baddour and N. C. Beaulieu, "Robust Doppler spread estimation in nonisotropic fading channels," *IEEE Trans. Wireless Commun.*, vol. 4, no. 6, pp. 2677–2682, Nov. 2005.

[13] C. Tepedelenlioğlu, A. Abdi, G. B. Giannakis, and M. Kaveh, "Estimation of Doppler spread and signal strength in mobile communications with applications to handoff and adaptive transmission," *Wireless Commun. Mobile Comput.*, vol. 1, no. 2, pp. 221–242, 2001.

[14] L. Krasny, H. Arslan, D. Koilpillai, and S. Chennakeshu, "Doppler spread estimation in mobile radio systems," *IEEE Commun. Lett.*, vol. 5, no. 5, pp. 197–199, May 2001.

[15] A. Dogandzic and B. Zhang, "Estimating Jakes' Doppler power spectrum parameters using the whittle approximation," *IEEE Trans. Signal Process.*, vol. 53, no. 3, pp. 987–1005, Mar. 2005.

[16] G. Lindgren, "Spectral moment estimation by means of level crossings," *Biometrika*, vol. 61, no. 2, pp. 401–418, 1974.

[17] A. Abdi and S. Nader-Esfahani, "Expected number of maxima in the envelope of a spherically invariant random process," *IEEE Trans. Inf. Theory*, vol. 49, no. 5, pp. 1369–1375, May 2003.

[18] H. Zhang and A. Abdi, "Nonparametric mobile speed estimation in fading channels: Performance analysis and experimental results," *IEEE Trans. Wireless Commun.*, vol. 8, no. 4, pp. 1683–1692, Apr. 2009.

[19] E. Stone and M. Skubic, "Evaluation of an inexpensive depth camera for passive in-home fall risk assessment," in *Proc. 5th Int. ICST Conf. Pervas. Comput. Technol. Healthcare*, May 2011, pp. 71–77.

[20] C. Zhang and Y. Tian, "RGB-D camera-based daily living activity recognition," *J. Comput. Vis. Image Process.*, vol. 2, no. 4, p. 12, 2012.

[21] H. Sakaino, "Video-based tracking, learning, and recognition method for multiple moving objects," *IEEE Trans. Circuits Syst. Video Technol.*, vol. 23, no. 10, pp. 1661–1674, Oct. 2013.

[22] L. Zhao, Z. He, W. Cao, and D. Zhao, "Real-time moving object segmentation and classification from HEVC compressed surveillance video," *Int. J. Adv. Res. Trends Eng. Technol.*, vol. 6, no. 12, pp. 1–8, Dec. 2019.

[23] P. Leusmann, C. Möllering, L. Klack, K. Kasugai, M. Ziefle, and B. Rumpe, "Your floor knows where you are: Sensing and acquisition of movement data," in *Proc. 12th Int. Conf. Mobile Data Manage. (MDM)*, vol. 2, 2011, pp. 61–66.

[24] R. Vera-Rodriguez, J. S. D. Mason, J. Fierrez, and J. Ortega-Garcia, "Comparative analysis and fusion of spatiotemporal information for footstep recognition," *IEEE Trans. Pattern Anal. Mach. Intell.*, vol. 35, no. 4, pp. 823–834, Apr. 2013.

[25] S. C. Mukhopadhyay, "Wearable sensors for human activity monitoring: A review," *IEEE Sensors J.*, vol. 15, no. 3, pp. 1321–1330, Mar. 2015.

[26] J. Bae and M. Tomizuka, "A tele-monitoring system for gait rehabilitation with an inertial measurement unit and a shoe-type ground reaction force sensor," *Mechatronics*, vol. 23, no. 6, pp. 646–651, Sep. 2013.

[27] *Run3D*. Accessed: Feb. 2020. [Online]. Available: http://www.run3d.co.uk/healthcare-professionals/about-our-run3d-system

[28] A. S. M. Sayem, S. Hon Teay, H. Shahariar, P. L. Fink, and A. Albarbar, "Review on smart electro-clothing systems (SeCSs)," *Sensors*, vol. 20, no. 3, p. 587, Jan. 2020.

[29] C.-Y. Hsu, Y. Liu, Z. Kabelac, R. Hristov, D. Katabi, and C. Liu, "Extracting gait velocity and stride length from surrounding radio signals," in *Proc. Conf. Hum. Factors Comput. Syst. (CHI)*, Denver, CO, USA, May 2017, pp. 2116–2126.

[30] Z.-P. Jiang, W. Xi, X. Li, S. Tang, J.-Z. Zhao, J.-S. Han, K. Zhao, Z. Wang, and B. Xiao, "Communicating is crowdsourcing: Wi-Fi indoor localization with CSI-based speed estimation," *J. Comput. Sci. Technol.*, vol. 29, no. 4, pp. 589–604, Jul. 2014.

[31] (2015). *Emerald*. [Online]. Available: http://www.emeraldforhome.com/s

[32] F. Adib, C.-Y. Hsu, H. Mao, D. Katabi, and F. Durand, "Capturing the coarse human figure through a wall," *ACM Trans. Graph.*, vol. 34, no. 6, Nov. 2015, Art. no. 219.

[33] Z. Yang, P. H. Pathak, Y. Zeng, X. Liran, and P. Mohapatra, "Monitoring vital signs using millimeter wave," in *Proc. 17th ACM Int. Symp. Mobile Ad Hoc Netw. Comput. MobiHoc (ACM)*, 2016, pp. 211–220.

[34] M. Wu, X. Dai, Y. D. Zhang, B. Davidson, M. G. Amin, and J. Zhang, "Fall detection based on sequential modeling of radar signal time-frequency features," in *Proc. IEEE Int. Conf. Healthcare Informat. (ICHI)*, Sep. 2013, pp. 169–174.

[35] B. Y. Su, K. C. Ho, M. J. Rantz, and M. Skubic, "Doppler radar fall activity detection using the wavelet transform," *IEEE Trans. Biomed. Eng.*, vol. 62, no. 3, pp. 865–875, Mar. 2015.

[36] M. G. Amin, Y. D. Zhang, F. Ahmad, and K. C. D. Ho, "Radar signal processing for elderly fall detection: The future for in-home monitoring," *IEEE Signal Process. Mag.*, vol. 33, no. 2, pp. 71–80, Mar. 2016.
[37] K. Qian, C. Wu, Z. Yang, Y. Liu, and K. Jamieson, "Widar: Decimeter-level passive tracking via velocity monitoring with commodity Wi-Fi," in *Proc. 18th ACM Int. Symp. Mobile Ad Hoc Net. Comp. (Mobihoc)*, Chennai, India, Jul. 2017, pp. 1–10.
[38] K. Qian, C. Wu, Y. Zhang, G. Zhang, Z. Yang, and Y. Liu, "Widar2.0: Passive human tracking with a single Wi-Fi link," in *Proc. 16th Annu. Int. Conf. Mobile Syst., Appl., Services (MobiSys)*, Munich, Germany, Jun. 2018, pp. 350–361.
[39] X. X. Li, S. Li, D. Zhang, J. Xiong, Y. Wang, and H. Mei, "Dynamic-music: Accurate device-free indoor localization," in *Proc. ACM Int. Joint Conf. Pervas. Ubiquitous Comput. (UbiComp)*, Heidelberg, Germany, Sep. 2016, pp. 196–207.
[40] X. Li, D. Zhang, Q. Lv, J. Xiong, S. Li, Y. Zhang, and H. Mei, "Indotrack: Device-free indoor human tracking with commodity Wi-Fi," in *Proc. ACM Interact., Mobile, Wearable Ubiquitous Technol. (IMWUT)*, New York, NY, USA, Mar. 2017, vol. 1, no. 3, pp. 1–22.
[41] S. Sen, J. Lee, K.-H. Kim, and P. Congdon, "Avoiding multipath to revive inbuilding Wi-Fi localization," in *Proc. 11th Annu. Int. Conf. Mobile Syst., Appl., Services (MobiSys)*, Jun. 2013, pp. 249–262.
[42] M. Kotaru, K. Joshi, D. Bharadia, and S. Katti, "SpotFi: Decimeter level localization using Wi-Fi," in *Proc. ACM Conf. Special Interest Group Data Commun. (SIGCOMM)*, Aug. 2015, pp. 269–282.
[43] D. Vasisht, S. Kumar, and D. Katabi, "Decimeter-level localization with a single Wi-Fi access point," in *Proc. 13th Symp. Netw. Syst. Design Implement. (NSDI)*, Mar. 2016, pp. 165–178.
[44] D. Umansky and M. Pätzold, "Design of measurement-based wideband mobile radio channel simulators," in *Proc. 4th Int. Symp. Wireless Commun. Syst. (ISWCS)*, Trondheim, Norway, Oct. 2007, pp. 229–235.
[45] A. Fayziyev and M. Pätzold, "An improved iterative nonlinear least square approximation method for the design of measurement-based wideband mobile radio channel simulators," in *Proc. Int. Conf. Adv. Technol. Commun. (ATC)*, Da Nang, Vietnam, Aug. 2011, pp. 106–111.
[46] A. Fayziyev and M. Pätzold, "The performance of the INLSA in comparison with the ESPRIT and SAGE algorithms," in *Proc. Int. Conf. Adv. Technol. Commun. (ATC)*, Hanoi, Vietnam, Feb. 2014, pp. 332–337.
[47] M. Naderi, M. Pätzold, and A. G. Zajić, "The design of measurement-based underwater acoustic channel simulators using the INLSA algorithm," in *Proc. Oceans*, Genova, NC, USA, May 2015, pp. 1–6.
[48] A. Abdelgawwad and M. Pätzold, "On the influence of walking people on the Doppler spectral characteristics of indoor channels," in *Proc. 28th IEEE Int. Symp. Pers., Indoor, Mobile Radio Commun. Workshops (PIMRC)*, Montreal, QC, Canada, Oct. 2017, pp. 1–7.
[49] R. Hicheri, M. Pätzold, and N. Youssef, "Estimation of the velocity of a walking person in non-stationary indoor environments from the received RF signal," in *Proc. IEEE 10th Latin-American Conf. Commun. (LATINCOM)*, Guadalajra, Mexico, Nov. 2018, pp. 1–6.
[50] R. Hicheri and M. Pätzold, "Estimation of the velocity of multiple moving persons in non-stationary indoor environments from received RF signals," in *Proc. IEEE 89th Veh. Technol. Conf. (VTC-Spring)*, Kuala Lumpur, Malaysia, Apr. 2019, pp. 1–7.
[51] J. E. Graham, S. R. Fisher, I.-M. Bergés, Y.-F. Kuo, and G. V. Ostir, "Walking speed threshold for classifying walking independence in hospitalized older adults," *Phys. Therapy*, vol. 90, no. 11, pp. 1591–1597, Nov. 2010.
[52] M. Pätzold and C. A. Gutierrez, "Modelling of non-WSSUS channels with time-variant Doppler and delay characteristics," in *Proc. IEEE 7th Int. Conf. Commun. Electron. (ICCE)*, Hue City, Vietnam, Jul. 2018, pp. 1–6.

RYM HICHERI (Member, IEEE) was born in Tunis, Tunisia, in 1988. She received the D.P.C.U. degree from the Institut Préparatoire Aux Etudes d'Ingénieurs d'El Manar, in 2009, and the Eng. degree in telecommunications and the Ph.D. degree in information and communication technology from the Ecole Supérieure des Communications de Tunis, Tunisia, in 2012 and 2017, respectively. She is currently a Postdoctoral Research Fellow with the University of Agder, Norway. Her current research interests include channel modeling, wireless communications, estimation and optimization, and information theory.

MATTHIAS PÄTZOLD (Senior Member, IEEE) received the Dipl.Ing. and Dr.Ing. degrees in electrical engineering from Ruhr University Bochum, Bochum, Germany, in 1985 and 1989, respectively, and the Habilitation degree in communications engineering from the Hamburg University of Technology, Hamburg, Germany, in 1998. From 1990 to 1992, he was with ANT Nachrichtentechnik GmbH, Backnang, Germany, where he was involved in digital satellite communications. From 1992 to 2001, he was with the Department of Digital Networks, Hamburg University of Technology. Since 2001, he has been a Full Professor of mobile communications with the University of Agder, Norway. He has authored several books and numerous technical articles. He has been actively participating in numerous conferences serving as a TPC member and the TPC Chair. His publications received 14 Best Paper Awards.

NÉJI YOUSSEF received the B.E. degree in telecommunications from the Ecole des Postes et des Télécommunications de Tunis, Tunisia, in 1983, the D.E.A. degree in electrical engineering from the Ecole Nationale d'Ingénieurs de Tunis, in 1986, and the M.E. and Ph.D. degrees in communication engineering from The University of Electro-Communications, Tokyo, Japan, in 1991 and1994, respectively. From 1994 to 1996, he was a Research Associate with The University of Electro-Communications. In 1997, he joined the Ecole Supérieure des Communications de Tunis, where he is currently a Professor. His research interests include noise theory, modeling of multipath fading channels, and performance analysis of wireless communications.